6

Multi-Channel Adaptive Interferometers Based on Dynamic Hologram Multiplexing

Roman Romashko and Yuri Kulchin
Institute of Automation and Control Processes FEB RAS
Russia

1. Introduction

Optical interferometry was always considered as one of the most flexible and sensitive techniques for measuring mechanical vibrations (Hariharan, 1990; Osterberg, 1932). The number of applications of this method tremendously increased after the discovery of lasers (in 1960) and the development of low-loss optical fibres (in 1966). A laser as a source of coherent radiation assures high sensitivity of an interferometer while an optical fibre guarantees compactness, light weight, immunity to electromagnetic influence, and capability of the measuring system to operate in hazardous conditions (high temperature, radiation, etc.). As known, the phase of a light field cannot be directly detected. It is an interferometer, which provides the detection of the phase difference by combining the signal wave (which bears information about the measurand) with the coherent reference wave and measuring changes of the resultant light flux by a photodetector. The sensitivity of an interferometer to phase difference is limited by shot noise of the photoelectrons and can be extremely high: the theoretical minimum detectable displacement (corresponding to the phase difference) is $1.1 \cdot 10^{-16}$ m $\cdot Hz^{-1/2}$ for 10 mW of detected laser power at the wavelength of 500 nm (Forward, 1978; Wagner & Spicer, 1987). However, two main problems should be overcome to achieve such high sensitivity in non-laboratory conditions. The first is the necessity of precise adjustment of the object and the reference wavefronts interfering at the photodetector. This requirement makes difficult, in particular, the use of multimode optical fibres in interferometric sensors. The second is the need to keep constant the average phase shift between the interfering wavefronts. This is more fundamental than the first one because the induced phase shift (which is assumed to be proportional to influence of the measurand on the optical paths) is nonlinearly transferred into the light-flux change at the detector via the familiar cosine interference function.

A simple and elegant solution of both these problems was achieved when a conventional beam-splitter, which serves for combining the reference and the object waves, was replaced by a dynamic hologram continuously recorded in a photorefractive crystal (PRC). Since the configuration in this case involves only two waves that interfere inside the crystal, it was called two-wave mixing, TWM (Huignard & Marrakchi, 1981). Considering that the photorefractive dynamic hologram adapts not only the signal wavefront to the reference one but it is also self-adapted to slow temporal variations of the phase difference, this type of optical system is referred to as adaptive interferometry (Stepanov, 1991). The idea of using

photorefractive crystals in an adaptive interferometer with multimode optical fibres was first proposed in 1980 by Hall et al. (Hall, et al., 1980). It was pointed out in this early paper that the physical mechanism of the dynamic grating formation in photorefractive crystals strongly affects phase-to-intensity transformation. The highest sensitivity to small phase excursions is achieved in the linear mode of phase detection when spatial variations of the refractive index inside the crystal are either non-shifted or shifted by a half of the grating period with respect to the interference fringes (Hall, et al., 1980). Such spatial shift occurs when the hologram is recorded in a photorefractive crystal under strong DC-field, in the so called drift regime (Young, et al., 1974). The main disadvantage of this approach is screening of the external electric field which leads to serious suppression of coupling of interfering beams in the illuminated part of the crystal. Another technical problem is overheating of the crystal under strong DC electric field. It is especially serious for fast photorefractive crystals because of their high photoconductivity. Strong overheating may even lead to the breakdown of the crystal. To prevent this DC-field should be applied to the crystal just during a short time (typically tens of milliseconds) followed by the relaxation period (typically tens of seconds). Thus the measurement can be done only in the pulse regime, which could be unacceptable for certain applications. Moreover, realization of this regime requires use of special synchronizing electronics that also complicates the measuring system as a whole. Alternatively, holographic recording in the diffusion regime (without external electric field) leads to the less sensitive, quadratic regime of phase demodulation (Kamshilin, et al., 1986). However, as it was shown later by Kamshilin and Grachev, the linear phase-to-intensity transformation can be achieved even in the diffusion regime of the hologram recording if the interfering waves have different polarization states (Kamshilin & Grachev, 2002). The last approach is based on vectorial-wave mixing (VWM) in photorefractive crystals for which the theory was developed by Sturman et al. (Sturman, et al., 1999). It is worth noting that an adaptive interferometer based on the technique proposed in (Kamshilin & Grachev, 2002) operates in so called enhanced diffusion mode when a strong AC-electric field is applied to a crystal for enhancing wave coupling. Further development of VWM-based approach has allowed one to find solutions which it made it possible:

- to avoid use of any external electric field due to recording the hologram in pure diffusion mode in reflection geometry of wave coupling at high spatial frequencies (Di Girolamo, et al., 2007a; Romashko, et al., 2005a);
- to use an object wave with arbitrary polarization (e.g. completely depolarized) without any polarization filtering, due to recording the hologram in orthogonal geometry of VWM (Di Girolamo, et al., 2010);
- to reduce significantly light intensity used for recording a dynamic hologram without worsening interferometer sensitivity and response time (Romashko, et al., 2007).

These solutions have allowed to significantly simplify the scheme of adaptive interferometer (by removing high-voltage suppliers, synchronizing feedback loops, etc.), improve performance stability, reduce optical loses, noise and energy-consumption. As a result, adaptive interferometers become more promising tools for different practical applications.

It is worth noting that nowadays the adaptive interferometers are intensively developed and find new and new application areas. First of all is non-destructive testing of materials and elements of technical constructions. In this area adaptive interferometry becomes one of the most promising techniques due to its possibility to operate reliably in an industrial

environment keeping the sensitivity at the high level approaching the classical homodyne detection limit. More specifically, adaptive interferometers are used in so-called laser ultrasound systems for non-destructive remote inspection of internal defects inside materials and constructions (Dewhurst & Shan, 1999). In these systems an acoustic wave (a sound pulse) generated by very short and powerful laser pulse propagates through a sample under the test and produces very week vibrations of the backside surface with the tiny amplitude of the order of 1 nm or even smaller. These vibrations (if they are detected by an adaptive interferometer) allow quality estimations of the tested object along the path of the sound pulse.

Another area of applications of phase demodulators based on photorefractive dynamic holograms is stabilization of fibre-optical interferometric sensors eliminating all unwanted influences of the environment (e.g., temperature changes) (Di Girolamo, et al., 2007a; Fomitchov, et al., 2002; Kamshilin, et al., 1995; Kamshilin, et al., 1998; Qiao, et al., 2006; Romashko, et al., 2005b). Adaptive interferometers find also application for real-time analysis of deformations and vibrations of technical constructions (such as space reflectors (Pauliat, et al., 2006) or even artworks (Thizy, et al., 2007)), for molecular recognition (Peng, et al., 2007), for acousto-optical imaging of biological tissues (Delaye, et al., 2005), for refractive index measurement (Lichtenberg, et al., 2005), in optical coherence-domain reflectometry systems (Peng, et al., 2003), and many others.

Among those applications there is a class of practical problems where several simultaneous measurements are required (Kulchin, 2001; Peiponen, et al., 2009). Thereby a development of multichannel adaptive system is a topical problem.

Taking into account that a key element of an adaptive interferometer is a dynamic hologram (DH) recorded in PRC, two possible strategies for development of multichannel systems can be considered. The first is based on using of several crystals, one for each channel. The advantage of this extensive approach is a possibility of providing complete independency of the system channels performance. However it leads to system complexity (due to the large number of reference beams, optical elements, etc.), disproportional increase of system cost, increase of energy consumption, reduced reliability and so on. An alternative strategy for development of a multi-channel adaptive interferometer consists in multiplexing of DHs in single PRC. Note that multiple holograms recording in same volume of photosensitive material is widely used for data storage in holography memory systems (Peiponen, et al., 2009; Steckman, et al., 2001), for correlation processing and pattern recognition (Feng, et al., 2000; Wen & Yang, 1997), in multichannel optical communication systems (An, et al., 2001; Petrov, et al., 2001), in multichannel measurement systems (Andersen, et al., 2009; Kujawinska & Robinson, 1988) and many others.

It is worth noting that static (or permanent) holograms can be multiplexed in a photosensitive material one by one. On contrary, a distinctive feature of both recording and reading out dynamic holograms is that the hologram disappears if light waves are switched off. Therefore a multiplexing of dynamic holograms is possible only in case of their simultaneous recording. This could leads to additional cross-talk between channels due to pair wise interaction of two arbitrary signal waves in the PRC. Moreover, an overlap of light fields from neighboring channels in a crystal volume could affect the parameters of the holograms and, as a consequence, the sensitivity of particular holographic channels. All these circumstances must be taken into account in the development of multichannel adaptive interferometric system.

All approaches for multiple hologram recording can be grouped into three classes: spatial, angular and spectral multiplexing techniques. In the first approach, holograms are recorded in different parts of the same crystal. This technique allows one to provide maximal independence of channel performance; the cross-talk is practically precluded. However, the number of multiplexed holograms (and therefore number of channels) is limited by the crystal size, and in most cases does not exceed a few tens (Kulchin, et al., 2000b). Moreover, an equivalent number of individual reference beams is required for recording of each hologram in this case, which also leads to complexity of the measurement system and brings its efficiency down.

Angular multiplexing of holograms allows significant increase in the number of channels formed in a single crystal. In this case the same volume of crystal can be used for recording several holograms, signal light beams can partially or even completely overlap in a crystal and a common reference beam can be used for all holograms. However cross-talk between channels becomes more probable in such a scheme. This defines one of the important problems which should be solved. It is necessary to find conditions which preclude a cross-talk between angular multiplexed holograms or the cross-talk level will be below the inherent noise of the system.

The spectral multiplexing approach is based on using different wavelengths for dynamic hologram recording. This approach naturally fits with the WDM-technique of fiber-optical sensors (especially FBG) multiplexing. As a result effective multichannel measurement systems can be created by combined these two principles. However a realization of the spectral multiplexing approach requires keeping a number of peculiarities. In particular, the spectral working range should match the spectral sensitivity of a photosensitive material (e.g. PRC). Moreover, it is necessary to take into account the possible appearance of cross-talk due to overlap of multiplexed channel spectra. The last requirement together with the first one constrains the number of channels which could be realized in a multichannel system based on spectral multiplexing.

Below in the following Sections 4-6 we consider more detailed practical realizations of multichannel adaptive interferometers and measurement systems based on the above listed principles of dynamic hologram multiplexing in a photorefractive crystal. First we give briefly the basics of wave mixing in photorefractive crystal (Section 2) and introduce a relative detection limit as a parameter which characterizes adaptive interferometer sensitivity (Section 3).

2. Two-wave mixing in photorefractive crystal: Vectorial model

The photorefractive (PR) effect known as light induced change of material refractive index was discovered in Bell Laboratory in 1966 (Ashkin, et al., 1966). In order to be photorefractive a material should have photoconductive and electro-optic properties. Then, in such a material, photo-induced charges migrate in the presence of light from regions of high optical intensity to regions of low optical intensity and eventually reach a static charge distribution. This charge distribution creates a strong, static electric field (so called space-charge field), which in turn alters the index of refraction of the material by the first-order electro-optic (Pockels) effect. Since its discovery in $LiNbO_3$ and $LiTaO_3$ the PR effect was observed in a great number of materials, including dielectrics, semiconductors, liquid crystals, organic polymers and even in liquids and gases.

The first theoretical model of the PR effect was proposed by Kukhtarev etal. in 1979 (Kukhtarev, et al., 1979). Later in 1999, Sturman et.al. developed more general and more rigorous theoretical model of two-wave mixing in PR crystal which takes into account a vectorial nature of light waves, anisotropic properties of photorefractive materials and anisotropy of light diffraction at a dynamic holographic grating (Sturman, et al., 1999).
After decades of studying the PR effect a number of fundamental monographs devoted to wave-mixing in PR materials were written (Petrov, et al., 1983; Petrov, et al., 1991; Solymar, et al., 1996; Sturman & Fridkin, 1992). These books can be recommended to the reader interested in detailed study of PR effect. In this Chapter we give just the main points of the theoretical model of vectorial wave mixing in PR crystal of cubic symmetry (Sturman, et al., 1999) which can help better understanding of further material.
Consider two coherent waves with vectorial amplitudes $\mathbf{A_1}$ and $\mathbf{A_2}$ entering a PR crystal of cubic symmetry under an external electric field $\mathbf{E_0}$ through its (*xy*)-face (Fig.1). In paraxial approximation valid for small angles between wave vectors $\mathbf{k_1}$ and $\mathbf{k_2}$ and axis *z* the wave amplitudes can be considered as 2D-vectors with *x*- and *y*-components.

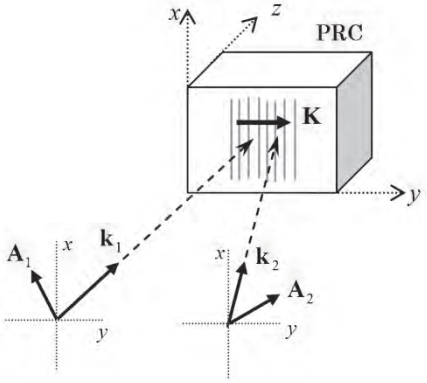

Fig. 1. Geometry of vectorial wave mixing in a photorefractive crystal

The waves' interference will result in the appearance of space charge field $\mathbf{E_K}$ which alters the crystal refractive index and forms a dynamic holographic grating with wave vector $\mathbf{K} = \mathbf{k_1} - \mathbf{k_2}$ in plane (*xy*). Diffraction of mixed waves at the dynamic grating provides their coupling which results in change of wave amplitudes at the crystal output. This process is described by the system of coupled-wave equations:

$$\begin{cases} \left(\frac{\partial}{\partial z}+\frac{\alpha}{2}-i\hat{\mathbf{G}}\right)\mathbf{A}_1 = iE_K\hat{\mathbf{V}}\mathbf{A}_2, \\ \left(g\frac{\partial}{\partial z}+\frac{\alpha}{2}-i\hat{\mathbf{G}}\right)\mathbf{A}_2 = iE_K^*\hat{\mathbf{V}}\mathbf{A}_1, \end{cases} \tag{1}$$

where *g* is the parameter which takes into account relative direction of wave propagation in the crystal (*g* = +1 in transmission geometry where waves propagate in same direction, and g = –1 in reflection geometry where waves propagate in opposite directions); α is the light absorption coefficient; E_K is the amplitude of space-charge field $\mathbf{E_K}$. Using the conventional one-trap–one-band model for the charge transfer (Petrov, et al., 1991) and assuming

provisionally that the applied field is parallel to the grating vector the space charge-field can be found, within the linear approximation in the contrast of the interference pattern, as

$$E_K = im\frac{(E_D + iE_0)E_q}{E_D + E_q + iE_0}, \tag{2}$$

where $m = 2\mathbf{A}_1\mathbf{A}_2^* / I_0$ is the contrast of the interference pattern, I_0 is the total light intensity, E_0 is the amplitude of external electric field applied to the crystal, while E_D and E_q are the characteristic fields,

$$E_D = \frac{Kk_BT}{e} \text{ (diffusion electric field), } E_q = \frac{eN_t}{\varepsilon\varepsilon_0 K} \text{ (traps saturation field),} \tag{3}$$

where e is the elementary charge, k_B is the Boltzmann constant, T is the absolute temperature, N_t is the effective concentration of photorefractive centers (traps), $\varepsilon\varepsilon_0$ is the dielectric constant. The matrices $\hat{\mathbf{G}}$ and $\hat{\mathbf{V}}$ are given by

$$G_{ij} = sE_0H_{ij}^{(0)} + i\rho\delta_{ijz}, \qquad V_{ij} = sH_{ij}, \tag{4}$$

here $s = -\pi n_0^3 r_{41} / \lambda$ is a material parameter; n_0 is the refractive index; r_{41} is the electro-optic coefficient; λ is the wavelength; ρ is the rotatory power; δ_{ijz} is the unit antisymmetric third rank tensor; $E_0 = |\mathbf{E_0}|$; $E_K = |\mathbf{E_K}|$. The Latin subscripts denote Cartesian components, and indices i and j assume independently the values x and y.

The tensors $\hat{\mathbf{H}}^{(0)}$ and $\hat{\mathbf{H}}$ responsible for electro-optic contribution to variation of crystal dielectric permittivity caused by external electric field $\mathbf{E_0}$ and internal space-charge field $\mathbf{E_K}$, are respectively:

$$H_{ij}^{(0)} = \frac{r_{ijl}E_{0l}}{r_{41}E_0}, \qquad H_{ij} = \frac{r_{ijl}E_{Kl}}{r_{41}E_K}, \tag{5}$$

where r_{ijl} is the electro-optic tensor. Taking into account that the space-charge field appears due to interference of mixed waves as well as a form of coupled-wave equations (1), one can conclude that tensor $\hat{\mathbf{H}}$ has the character of the wave-coupling matrix. The last becomes more clear in the case of waves mixing in non-gyrotropic crystal ($\rho = 0$) without application of external electric field ($E_0 = 0$) when the system (1) is reduced to the following

$$\begin{cases} \left(\frac{\partial}{\partial z} + \frac{\alpha}{2}\right)\mathbf{A}_1 = smE_K\hat{\mathbf{H}}\mathbf{A}_2, \\ \left(g\frac{\partial}{\partial z} + \frac{\alpha}{2}\right)\mathbf{A}_2 = -smE_K\hat{\mathbf{H}}\mathbf{A}_1. \end{cases} \tag{6}$$

As seen from Eqs.(6) in order for the waves to couple they must interfere ($m \neq 0$) with matrix $\hat{\mathbf{H}}$ being non-zero.

By solving Eqs.(1), one can find amplitudes of mixed waves at the output of the PR crystal. Note that a particular solution depends on wave mixing geometry which, in its turn, is

determined by the orientation of holographic grating vector, **K,** and the directions of wave propagating (vectors $\mathbf{k_1}$ and $\mathbf{k_2}$) with respect to crystallographic axes of the crystal (Romashko, et al., 2010; Sturman, et al., 1999).

It is worth noting that the particular type of the matrix $\hat{\mathbf{H}}$ is closely related to the type of light diffraction at a dynamic hologram. Thus, in the case of pure isotropic diffraction which preserves the polarization of the diffracted light, the coupling matrix is proportional to the unit matrix, $\hat{\mathbf{H}} = const\hat{\mathbf{1}}$. In all other cases the diffraction is anisotropic and is accompanied by change of diffracted light polarization state. Particularly if the polarization plane of diffracted wave is rotated by 90 degrees with respect to the incident light the matrix is $\hat{\mathbf{H}} = \begin{pmatrix} 0 & 1 \\ 1 & 0 \end{pmatrix}$. The last case is considered as most efficient for providing a linear regime of phase demodulation in the adaptive interferometer based on a dynamic hologram recorded in PR crystal in diffusion mode, i.e. without application of external electric field (Kamshilin, et al., 2009).

3. Adaptive ineterferometer sensitivity

Since in any interferometer a physical parameter, which has to be measured, is finally encoded in the phase modulation of the light wave, its sensitivity to small phase excursions is a parameter serving as a primary criterion for comparison of different systems. It is not only the configuration of the optical scheme but also its particular realisation (the output laser power, the generated wavelength, the type of the crystal, etc.) which determines the sensitivity of an adaptive interferometer. Comparison of different adaptive interferometers is usually done by estimation the extent to which their sensitivity is worse than that of the classical lossless interferometer (Delaye, et al., 1997; de Montmorillon, et al., 1997). It was shown in early papers devoted to analysis of a classical interferometer that its sensitivity can be extremely high if the available light power is not limited and measurements of the phase modulation is carried out within a very narrow frequency band (Bershtein, 1954; Forward, 1978). Evidently, the minimum detectable phase difference $\Delta\phi^{min}$ is defined by the noise level of the measuring system. There are several sources of the noise in an optical interferometer: laser noise, thermal and shot noise of the photodetector, and noise of amplifying electronics. When the light power arriving at the photo-detector is high enough, shot noise (which is proportional to the square root of the received light power) of the photo-excited charge carriers prevails over all the other noise levels (Bershtein, 1954; Wagner & Spicer, 1987). The shot noise is the instability of the photodetector current caused by statistical fluctuation of the number of received photons. Its level is primarily defined by the average number of photons and it is given as:

$$\left\langle i_{shot}^2 \right\rangle = 2\frac{e^2\eta}{h\nu}\langle P_D \rangle \Delta f \ , \tag{7}$$

where e is the electron's charge, η is the quantum efficiency of the photo-detector, $h\nu$ is the energy of the photon, and Δf is the frequency bandwidth of the detection electronics.

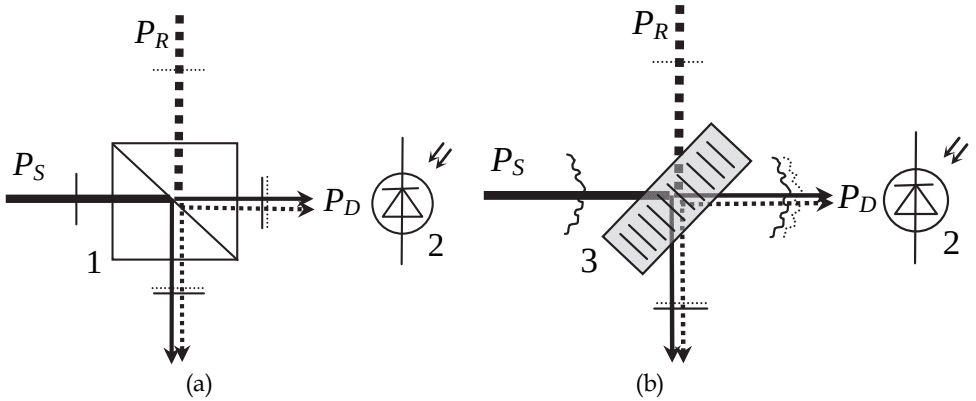

Fig. 2. Combining the signal (P_S) and the reference (P_R) waves using the conventional beam-combiner in the classical interferometer (a) and the dynamic hologram of an adaptive interferometer (b): 1 – the beam combiner; 2 – the photodetector; 3 – the photorefractive crystal

Let us now calculate the signal-to-noise ratio for phase demodulation in the classical interferometer, which is schematically shown in Fig. 2(a). As is known, the highest sensitivity of the interferometer is achieved at the quadrature condition, when the average phase difference between the interfering beams is equal to $\pi/2$ (Osterberg, 1932). When we introduce a small phase difference, $\Delta\phi$, the light power arriving at the photo-detector is

$$P_D = \frac{1}{2}\left(P_S + P_R\right) + \sqrt{P_S P_R}\,\sin\Delta\phi \approx P_S\frac{1+\beta}{2} + P_S\sqrt{\beta}\cdot\Delta\phi\,, \tag{8}$$

where P_R and P_S are the power of the reference and object wave, respectively, β is their ratio. Here we neglected all optical losses and assumed that the cross-sections of the interfering beam are the same. The informative signal in the interferometer is the electric current of the photodetector proportional to $\Delta\phi$. Assuming linear response of the photodetector to the incoming light power P_D, the signal is directly proportional to the second term in Eq. (8), while the first term is responsible for the shot noise given by Eq.(7). Therefore, the signal-to-noise ratio achieved in the classical interferometer is

$$SNR_C = \frac{\Delta\phi}{Q}\sqrt{\frac{2P_S}{1+\beta^{-1}}}\,, \quad \text{with} \quad Q = \sqrt{\frac{4h\nu\Delta f}{\eta}}\,. \tag{9}$$

The minimum detectable phase difference (the classical homodyne detection limit), $\Delta\phi_C^{min}$, is usually defined as the phase shift, which leads to $SNR = 1$. For large beam intensity ratio ($\beta >> 1$) Eq. (9) yields

$$\Delta\phi_C^{min} = \sqrt{\frac{2h\nu\Delta f}{\eta P_S}}\,. \tag{10}$$

Performance of any adaptive interferometer, which is schematically shown in Fig. 2(b), is conveniently compared with the performance of the classical interferometer by introducing the parameter

$$\delta_{rel} = \frac{\Delta\phi_A^{min}}{\Delta\phi_C^{min}} = \frac{SNR_C}{SNR_A}, \tag{11}$$

which can be called the relative detection limit. In Eq. (11) $\Delta\phi_A^{min}$ is the minimal detectable phase difference in the adaptive interferometer and SNR_A is the signal-to-noise ratio achieved in the adaptive interferometer by introducing the phase shift of $\Delta\phi$. On the one hand, the relative detection limit, δ_{rel}, is the ratio of the detection limits of both interferometers. On the other hand, it shows how the response of the classical interferometer to a known phase difference $\Delta\phi$ is larger than that of the adaptive interferometer.

Correct comparison of the adaptive and classical interferometers can be carried out if we use the same power of the object beam, the same photodetector and electronic circuit, and the same phase difference between the interfering beams. If the performance of the adaptive interferometer is analytically described, the relative detection limit can be calculated theoretically. Alternatively, δ_{rel} can be measured in the experiment as follows. Suppose that introduction of the small phase difference of $\Delta\phi$ in the adaptive interferometer results in a change of the light power at the photodetector by ΔP_D but the mean power, $<P_{D0}>$, remains the same. In this case the signal-to-noise ratio of the adaptive interferometer is

$$SNR_A = Q^{-1}\frac{\Delta P_D}{\sqrt{P_{D0}}}. \tag{12}$$

The light power P_{D0} is certainly related to the incident power P_S as $P_{D0} = P_S\Im$, where $\Im$ is the system transmission, which takes into account the optical losses in the crystal and all other optical elements ($\Im \le 1$), which is readily measured in the experiment. By introducing Eqs. (9) and (12) into Eq. (11), we get for $\beta >> 1$:

$$\delta_{rel} = \sqrt{\frac{2}{\Im}}\frac{P_{D0}}{\Delta P_D}\Delta\phi. \tag{13}$$

The relative detection limit is always larger than unity and it increases for higher optical losses (when $\Im$ decreases). The ratio $\Delta P_D / P_{D0}$ is readily measured because it is equal to the ratio of the modulated part of the photodetector current to its non-modulated part (i.e., to visibility of an oscilloscope trace when the small phase excursion of $\Delta\phi$ is applied to interferometer. Other parameters of equation (13) can be also readily estimated in the experiment. Therefore, Eq. (13) provides easy way to measure the relative detection limit δ_{rel}. This parameter is very convenient for comparison of different adaptive interferometers. Moreover, it also allows us to estimate the minimal detectable phase shift $\Delta\phi_A^{min}$ for the particular adaptive interferometer as $\Delta\phi_A^{min} = \delta_{rel}\Delta\phi_C^{min}$.

In following Sections we consider different schemes for multichannel adaptive interferometers based on spatial, angular and spectral multiplexing of dynamic holograms in a photorefractive crystal.

4. Spatial multiplexing of dynamic holograms

A multichannel adaptive interferometric demodulator proposed in (Kulchin, et al., 2000b) is built using the spatial multiplexing of dynamic holograms which are recorded in $Bi_{12}TiO_{20}$ crystal in its different parts (Fig.3). The holographic demodulation channels operate on the basis of the so called fanning effect (Voronov, et al., 1980) which appears as self-diffraction of light wave in photorefractive media. The nature of this effect consists in energy transfer between light beam entered the photorefractive crystal and beams scattered by crystal defects and inhomogeneities (Feinberg, 1982). Interference of initially weak scattered beams with the injected beam forms a set of dynamic holographic gratings. Diffraction of the input beam by these holograms leads to enhancement of those scattered waves which satisfy the phase-matching condition (Cronin-Golomb & Yariv, 1985). Due to holographic nature of fanning effect, any fast modulation of the phase of the injected light wave results in a variation of scattered light intensity; so the demodulation signal appears. Figure 4 illustrates light intensity distribution (fanning light) at the output of crystal when two holographic demodulation channels are formed. The channels optical beams are so close in a crystal that fanning waves are completely overlapped in the near field (Fig.4(a)) and can be separated only in the far field (Fig.4(b)), where they can be independently measured.

The authors show that demodulation signal in a channel decreases if the distance between light beams associated with multiplexed channels becomes below the lateral dimension of a channel (beam diameter) d (Fig.5). Such depletion is caused by reduction of interference pattern contrast m in a channel when light from another channel gets inside it. However this depletion is not critical – the output signal level reduces only by 2.5 dB even if optical fields from multiplexed channels completely overlap ($x = 0$).

Both the peculiarity and the advantage of holographic channel performance on the base of fanning effect are related to the fact that holograms are formed in a crystal without an external reference beam – the light waves scattered at the crystal defects act as a reference waves. Therefore radiation in a particular channel can be mutually non-coherent with other channels. Due to this, overlap of light waves from different channels does not lead to formation of cross-holograms and, as a sequence, does not produce cross-talk between channels. Figure 5 shows dependency of demodulation signal in 1st channel tuned to the

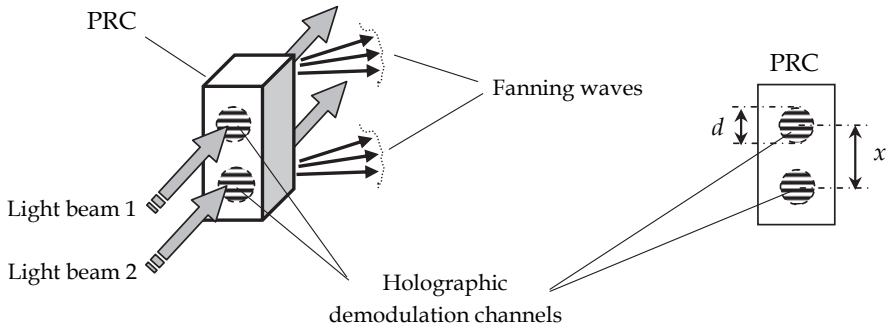

Fig. 3. Multi-channel adaptive demodulator based on spatial multiplexing of dynamic holograms in a photorefractive crystal: d is the characteristic dimension of a channel defined by light beam spot diameter, x is the distance between channel centers

frequency of 2nd channel on relative distance between channels. As seen this signal does not depend on channels overlapping ratio, while its level does not exceed the inherent noise level of a channel (– 11 dB).

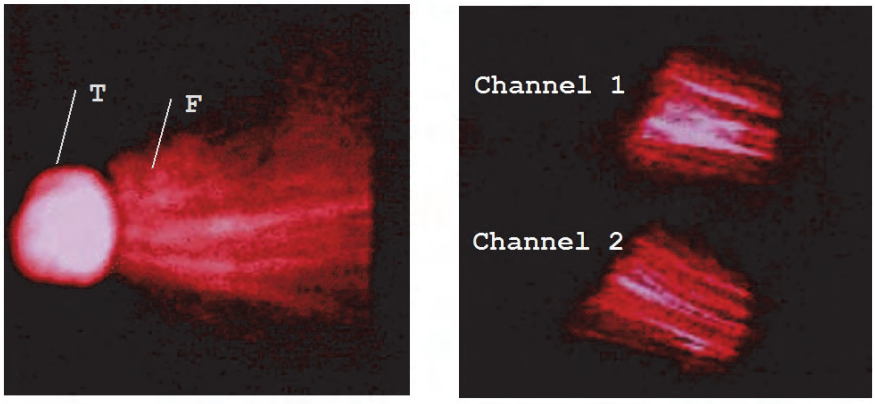

(a) (b)

Fig. 4. Photographs of light field at the output of PR crystal in which two holographic channels are created: (a) near field image (T –beam transmitted through the crystal; F – fanning waves), (b) far field image of fanning waves (transmitted beam is blocked)

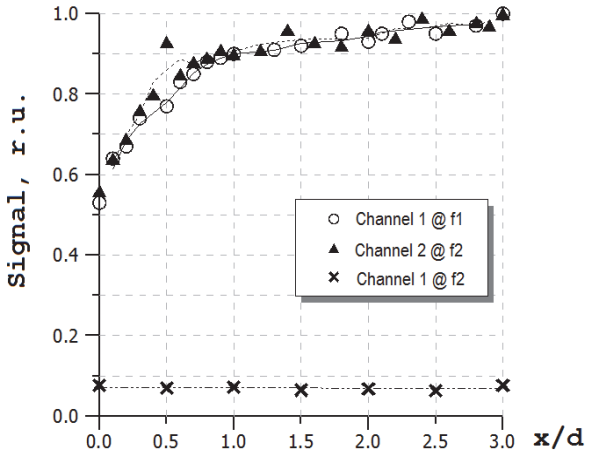

Fig. 5. Dependency of demodulation signals in two channels multiplexed in PR crystal on the relative distance between them. Channels provide processing of optical signals from two fiber-optical sensors detecting vibration at two different frequencies f_1 and f_2. The signal level in 1st channel tuned the frequency of 2nd channel does not exceed noise level of detection electronic equipment, which demonstrates the practical absence of cross-talk between channels

(a) (b)

Fig. 6. Photographs of fanning waves at the output of two-channel holographic demodulator formed in PR crystal when a mechanical impact under measurement is applied to a sensor and is detected in the 1st channel (a) and in the 2nd channel (b)

Figure 6 shows photographs recorded in the far field of fanning waves intensity distribution for the case of two holographic channels multiplexed in BTO crystal. The distance between channels in a crystal is equal to a channel radius (x/d = ½), providing partial overlap of channel light fields. The radiation entering the crystal is coming from two independently operated fiber-optical sensors – single-fiber multimode interferometers which have speckled waves at their outputs (Kulchin, 2001). When one of sensors remained quiet, the other one was exposed to a sudden impact with amplitude sufficient for rearrangement of speckle pattern and, as consequence, to diminishing of fanning wave intensity in the corresponded channeling (Fig.6). At the same time the level of fanning wave intensity in the rest channel remained constant. This result demonstrates the independence of fanning-effect-based channels operation even in the case of significant overlap of channel light fields in the bulk photorefractive crystal.

The two-channel adaptive fiber-optical measurement system based on the considered multichannel holographic demodulator was tested for monitoring of cracks formation in an object under increasing mechanical stress (Kulchin, et al., 2000a). Two fiber-optical sensors based on multimode fibers were first embedded into the structure of the test object when it was created (see Fig.7). Mechanical stress caused by gradually increasing pressure applied to the object led to initiation of cracks whose appearance is accompanied by generation of sound pulses. In their turn sound pulses propagating in the object affect the optical fibers and modulate the phase of optical radiation guided by fibers. Phase demodulation is performed by means of dynamic holograms multiplexed in PRC. Figure 8 shows oscilloscope traces of demodulated signals in two channels.

It is worth noting that the adaptive property of a holographic demodulator formed in PRC allows not only protection of a measurement system from the influence of the environment (temperature drift, pressure variation, etc.) but also makes it insensitive to slow deformation of the object, providing a detection of only those moments in time when cracks appear.

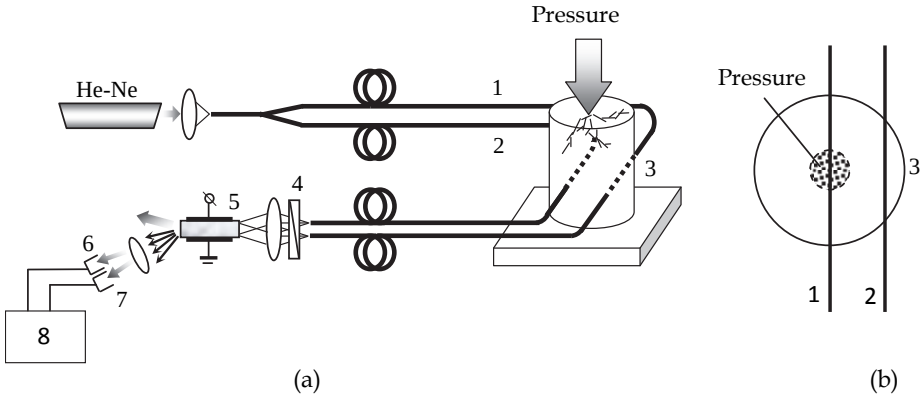

Fig. 7. Two-channel adaptive fiber-optical measurement system (a) and layout of sensing optical fibers in the object under the test – top view (b): 1, 2 – optical fibers; 3 – test object; 4 – polarizer; 5 – PR crystal $Bi_{12}TiO_{20}$; 6, 7 – channels photodetectors; 8 – recording system

As seen from the signal traces, crack frequency increases with growing of object deformation. It is more typical for the center part of the object where external pressure is applied and where the fiber #1 is placed (see Fig.7(b)). The object being stressed was broken at 325th second. The fiber placed in the center was broken together with the object. As a result the signal disappeared in the first channel. The second fiber remaining unbroken still detects weak signals indicating cracks which appear now in the object fragments. Start from 370th second, the press machine which creates mechanical stress in the object powders its central part thus stopping cracks formation process.
As seen from the oscilloscope traces, both channels operate independently without any detectable cross-talk.

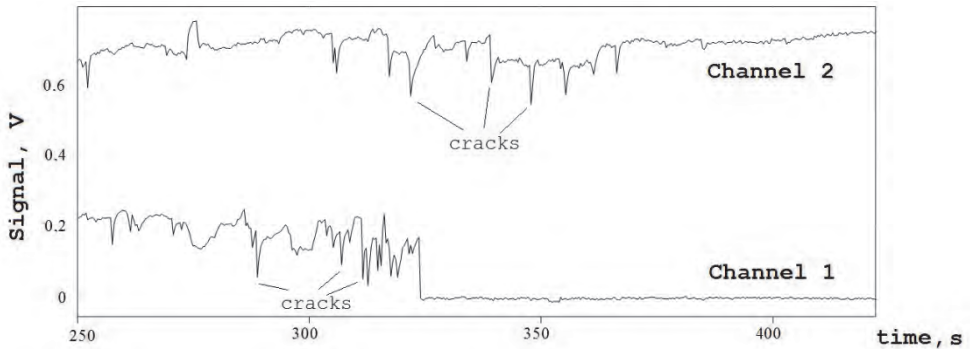

Fig. 8. Oscilloscope traces of photodetector signals in two channels of an adaptive fiber-optical measurement system which monitors crack the formation process in a solid state object

5. Angular multiplexing of dynamic holograms

The authors of paper (Fomitchov, et al., 2002) realized a multi-channel measurement system on the basis of angular multiplexing of dynamic holograms in a photorefractive crystal. The

scheme of the multichannel holographic demodulator is shown in Fig.9. Several signal waves coming from fiber-optical sensors which transform a measurand (ultrasound waves) to light phase modulation are directed to the photorefractive crystal $Bi_{12}SiO_{20}$ where they are mixed with a common reference wave. Pair wise interference of all signal waves with the reference one forms a set of main dynamic holograms which provide phase demodulation of the corresponding signal waves.

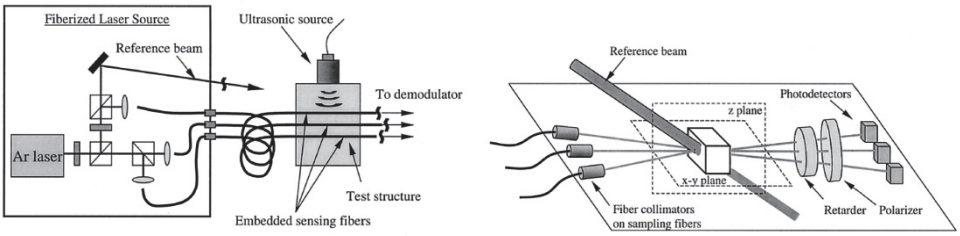

(a) (b)

Fig. 9. Optical schematic of laser source and typical arrangement of sensing fibers (a) and three-channel adaptive demodulator based on angular multiplexing of dynamic holograms in BSO crystal (b)

Use of a common reference beam for all multiplexed holograms implies that all signal waves are mutually coherent. In this case, overlap of signal beams could lead to formation of cross holograms and, as a sequence, to appearance of cross-talk between multiplexed holographic channels. In order to minimize the effect of cross holograms and to reduce a cross-talk the following approach is used. As seen from Fig.9 the holograms are recorded in so called transmission geometry – all mixed beams propagate in the crystal in same direction at small angles to each other. Having large spatial period Λ (or small wave number, $K = 2\pi / \Lambda$) the holographic grating has low diffraction efficiency which is defined by space charge field E_K proportional to K in accordance with Eqs.(2)-(3). In order to enhance the wave coupling efficiency in transmission holograms a strong external electric ac field with amplitude E_0 = 6 kV/cm and frequency 3000 Hz was applied to the PRC. Meanwhile the geometry of beams propagating in the crystal has provided mutual orthogonality of grating vectors of main and cross-holograms (see Fig.10). Indeed, the incidence plane (xy) of signal beams forming cross-holograms is orthogonal to the incidence plane (yz) of the reference beam which forms the main holograms. Thus, an external electric field applied to the crystal along grating vectors of main holograms has provided enhancement of their diffraction efficiency (see Eq.(2)), while cross-holograms remained unamplified. Moreover the angle between any pair of signal beams is much smaller than that between any signal and reference beams. This makes the cross-holograms weaker in comparison with the main holograms, thus reducing the cross-talk between channels

The three-channel adaptive measurement system based on the above considered approach of dynamic holograms angular multiplexing was applied to the detection of ultra-sound pulse propagation in a composite structure material (CSM). Three sensing fibers were embedded between CSM layers as shown in Fig.11(a). A 5-MHz contact transducer was used to launch bulk waves into the composite. The ultrasonic wave packet was detected by the sensing fibers, which were located at different depths within the composite.

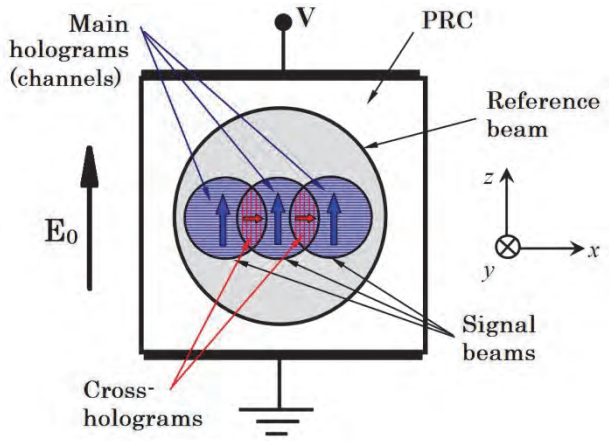

Fig. 10. Geometry of multi-wave mixing in PRC providing angular multiplexing of transmission dynamic holograms: all signal waves belong to horizontal plane (*xy*) and propagate in direction close to axis *y*; the reference wave belongs to plane (*yz*) and makes the angle of 5° with plane (*xy*)

The normalized ultrasonic signals are shown in Fig. 11(b). From the measured signals it can be seen that the bulk longitudinal waves are clearly detected by all three channels with good sensitivity. The longitudinal wave arrives at different times at different sensor locations, providing information about the wave speed (related to material properties of the composite). The measured longitudinal velocity of 2480 m/s agrees well with data obtained for the same composite material by a different technique (Fomitchov, et al., 2001). Furthermore, the absence of any spurious signals in sensors 2 and 3 at the time of arrival of the ultrasonic wave packet at sensor 1 is an indication of the absence of cross-talk in the multichannel adaptive system based on dynamic holograms multiplexed in a PR crystal.

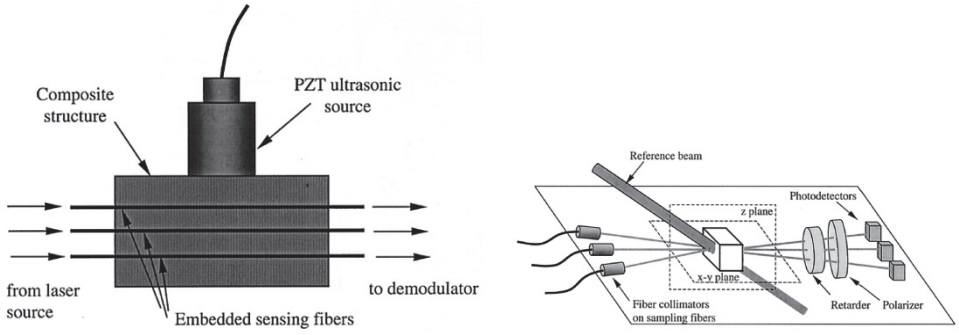

Fig. 11. (a) Experimental arrangement used to detect bulk ultrasonic waves in a composite sandwich structure, (b) detected ultrasonic signals for all three channels

In spite of such a satisfactory performance the system proposed in (Fomitchov, et al., 2002) has a major drawback. This is the necessity of using strong external electric field which leads

to the technical problems common to all systems based on drift recorded dynamic holograms mentioned in the Introduction. Moreover, in order to realize a linear regime of phase demodulation the retarder plate installed after the crystal is used together with polarizer which introduces optical losses and produces polarization noise (Di Girolamo, et al., 2007b). In its turn, it was shown in the paper (Di Girolamo, et al., 2007a) that high efficiency of dynamic hologram (and, as sequence, high sensitivity of adaptive interferometer) can be achieved even without any external electric field if the hologram is recorded in reflection geometry at high spatial frequencies, *K*. Moreover, the linear mode of phase demodulation can be realized in this case also without any polarization filtering – due to VWM of waves with different polarization states (e.g., linear and elliptical) in a geometry which supports anisotropic diffraction of light (see Section 2). As was shown further in our paper (Di Girolamo, et al., 2008) a multiplexing of diffusion dynamic holograms of the reflection type can became a basis for an efficient multi-channel adaptive measurement system. Consider this approach in more details.

The geometry of reflection holograms multiplexing in a PR crystal of cubic symmetry is shown in Fig.12. Two signal waves S_1 and S_2 propagate in the crystal along its principal crystallographic axis [001] and mix with the reference wave R propagating in the opposite direction toward to them. As in the previous case, all mixed waves are mutually coherent. Thus their pair wise interference can lead in general to formation of dynamic holograms of two kinds – (i) the main DHs recorded by a reference and a signal beam and (ii) cross holograms recorded by pair of signal beams. The main holograms form demodulation channels while the presence of cross-holograms can become a source of cross-talk between channels. Moreover, the multiple recording of DHs in a single crystal can lead in general to reduction of diffraction efficiency of a particular dynamic hologram and, as sequence, to depletion of the sensitivity in particular channel. Both the rate of sensitivity decrease and the cross-talk level determine the performance of a multi-channel holographic demodulator. Consider this in more details.

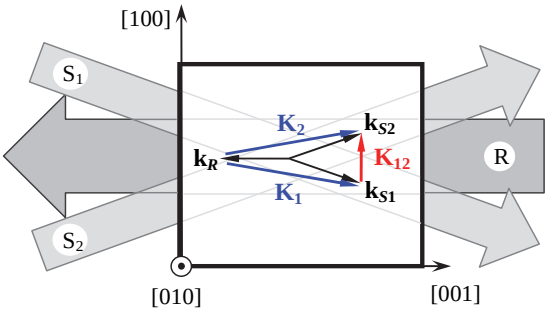

Fig. 12. The geometry of multiplexing of two reflection dynamic holograms in a PR crystal: $\mathbf{k}_R, \mathbf{k}_{S1}, \mathbf{k}_{S2}$ are wave vectors of reference (R) and signal (S_1, S_2) light waves, respectively; $\mathbf{K}_1, \mathbf{K}_2$ are grating vectors of main holograms; $\mathbf{K}_{12}$ is the grating vector of cross-hologram

Recall that two-wave mixing in PR crystal is described by system of coupled-wave equations (1) or (6) where $\hat{\mathbf{H}}$ is the coupling matrix whose components are determined by the orientations of the grating vector and wave propagation directions with respect to the

crystallographic axis (see Eq.(5)). One can show that for the geometry depicted in Fig.12 the matrix $\hat{\mathbf{H}}$ has non-zero components ($\hat{\mathbf{H}} = \begin{pmatrix} 0 & 1 \\ 1 & 0 \end{pmatrix}$) only for counter propagating waves coupled at hologram by the grating vector parallel to the principal crystallographic axis [001]. As seen in Fig.12 this requirement is satisfied for any pair of signal and reference waves.

On the contrary, the grating vector $\mathbf{K_{12}}$ of the cross-hologram formed by any pair of two signal waves is orthogonal to the axis [001]. By using Eq.(5) one can show that all components of the coupling matrix $\hat{\mathbf{H}}$ in this case will be zero, $\hat{\mathbf{H}} = \begin{pmatrix} 0 & 0 \\ 0 & 0 \end{pmatrix}$. This means that, in such geometry, there is no coupling between signal waves even if they completely overlap, and hence there is no cross-talk between channels associated with these signal waves.

However the situation changes if the orthogonality of a cross-hologram grating vector $\mathbf{K_{12}}$ to direction [001] is violated (this becomes true if signal beams enter the crystal at different angles). Thus the efficiency of two signal waves coupling in this case will depends on the [001]-axis component of the vector $\mathbf{K_{12}}$. Taking into account that the efficiency of waves mixing at the main hologram (and hence the level of demodulation signal in a channel) is determined by wave number K (i.e. K_1 or K_2) in accordance with Eq.(3), one can show that the cross-talk level can be estimated with good accuracy by following

$$C \approx 20\log\left(h\frac{|\sin\Theta|}{2}\right), \tag{14}$$

where Θ is the angle between vector $\mathbf{K_{12}}$ and normal to axis [001], $h \le 1$ is the coefficient which takes into account degree of signal beams overlap in a crystal.

Figure 13 shows the dependency $C(\Theta)$ from which it is seen that violation of orthogonality $\mathbf{K_{12}} \perp [001]$ leads to a rise in cross-talk. However, its level remains below the inherent noise of a channel (–30 dB) over a wide range of angles Θ. The last provides wide angular aperture for entry of signal beams to a crystal (Fig.14). Thus, for the CdTe crystal having refractive index ~2,8 the aperture within which a cross-talk is practically absent can reach 60 degrees. Moreover the signal beams can belong to different planes (e.g., spaced in fantail way) in contrast to the previous multiplexing technique where they lay in same plane, see Fig.9(b). The wide angular range of signal beams input makes the formation of holographic channels easy and increases their potential number.

As it was shown in the paper (Di Girolamo, et al., 2008) another possible reason for cross-talk in the geometry of reflection holograms multiplexing is related to residual mechanical stresses or defects in PR crystal which locally disturb its symmetry and partially enable interaction of signal beams even in forbidden geometry (when $\mathbf{K_{12}} \perp [001]$). In this case matrix $\hat{\mathbf{H}}$ can have non-zero components. However the cross-talk level still does not exceed channel inherent noise. A low level of cross-talk is obtained by low spatial frequency of cross hologram grating K_{12} which is much smaller than that of main holograms, K_1 and K_2. It worth noting that cross-talk related to crystal defects/stresses can be excluded (or at least minimized) by using crystals of better quality.

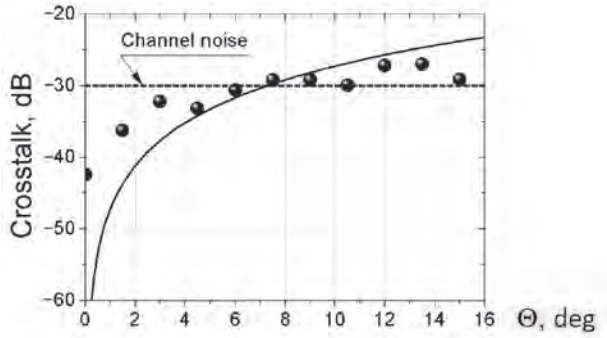

Fig. 13. Cross-talk between channels as function of angle between cross-hologram grating vector and normal to the crystal axis [001]: line represents theoretical dependency calculated in accordance with Eq.(14); markers are experimental data

As seen from Eqs.(2), (6), the efficiency of wave coupling at a dynamic hologram (and hence demodulation signal amplitude) is defined by the interference pattern contrast $m = 2\mathbf{A}_1\mathbf{A}_2^* / I_0$. However this expression is valid only for the two-wave mixing case. Introduction of additional signal waves (related with other channels) changes the contrast.

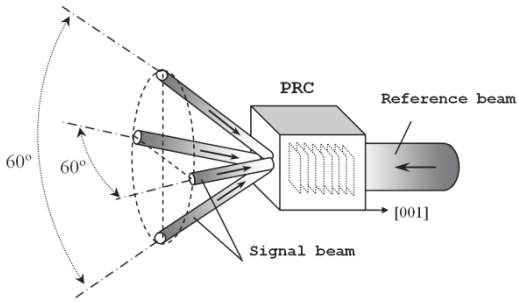

Fig. 14. Spatial arrangement of beams providing multiple recording of reflection dynamic holograms in a photorefractive crystal without noticeable crosstalk

In spite of mutual coherence of all light beams crossed in the crystal, the change of contrast is related mostly to increase of total light intensity. High angular selectivity of volume holograms allows one to exclude contributions to the variable part of the contrast from additional interference patterns having spatial frequencies and orientation different from those of main hologram. Thus the contrast of the interference pattern in the one of N channels can be estimated by

$$m(N) = \frac{2\sqrt{I_S I_R}}{I_R + I_S + h\sum_{j=1}^{N-1} I_j}, \tag{15}$$

where I_R , I_S and I_j are the intensities of reference beam, signal beam of a particular channel and signal beam of the j-th additional channel, respectively.

It is worth noting that maximum sensitivity of an adaptive interferometer based on a dynamic hologram is achieved at a certain ratio of mixed beam intensities (Di Girolamo, et al., 2008). Thus, taking into account that a common reference beam is used in the considered geometry of hologram multiplexing the optimized multichannel system will have signal beams of equal intensity, $I_j = I_S, (j = 1, N)$. Then, Eq.(15) for contrast of interference pattern in one of N multiplexed channels can be reduced with good accuracy to the following

$$m(N) \approx \frac{2\sqrt{I_S I_R}}{I_R + hNI_S}. \tag{16}$$

By solving the system of coupled wave equations (1) talking into account Eq.(16) one can analyze one channel performance under conditions of decreasing number of channels. Figure 15 shows dependency of the relative detection limit δ_{rel} on multiplexed channels number N. As seen, increase of N is accompanied by increase of detection limit (equivalent to reduction of sensitivity, see Eq.(11)) in each channel. However this increase is not critical and depends on the crystal sample. Thus, formation of 10 channels in one sample of CdTe crystal leads to doubling of δ_{rel} while for another sample of same crystal this increase amounts to just 23%. Taking into account the extremely high sensitivity of an adaptive interferometer which approaches that of classical interferometer (Kamshilin, et al., 2009), one can conclude that even a reduction of sensitivity by a factor of two can be considered as not significant and remains acceptable in most practical applications. Additionally mutual influence of multiplexed channels can be diminished by reduction of the degree of signal beams overlap h (see Eq.(15)) using their tighter focusing.

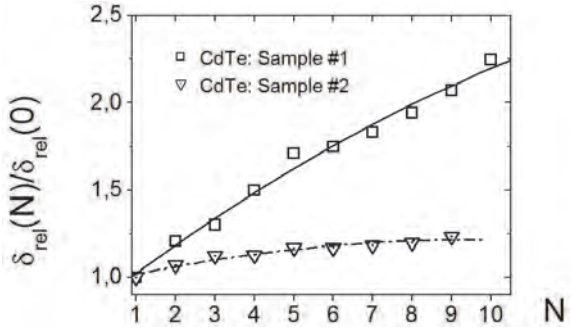

Fig. 15. Dependence of relative detection limit in one channel of holographic multi-channel system on number of multiplexed channels

The scheme of a two-channel adaptive interferometer based on angular multiplexing of reflection dynamic holograms in a photorefractive crystal CdTe in the above-considered geometry is shown in Fig. 16. Two signal beams coming from two sensing optical fibers are focused by lenses into the crystal where they are mixed with a reference beam propagating in the opposite direction along the crystallographic axis [001]. Calibrated piezoelectric transducers attached to the fibers simulate the action of measurand and introduce phase modulation with amplitudes 0.30 and 0.15 rad in the first and the second channels, respectively. This is equivalent to a detection of mechanical vibration with amplitude of 25

and 13 nm (at wavelength 1.06 μm), respectively. Oscilloscope traces of detected signals in two channels of the adaptive interferometer are shown in Fig.17. As seen the measurement system provides good SNR in both channels in spite of the weak level of measured vibration and wide-band detection mode (Δf = 50 MHz). Moreover, the two channels operate independently without any detectable cross-talk.

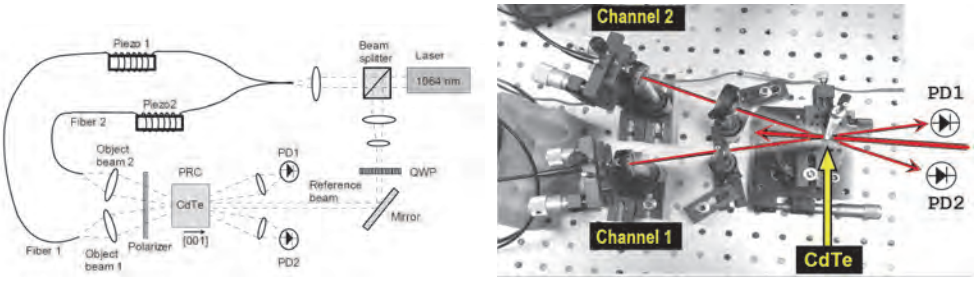

(a) (b)

Fig. 16. Layout (a) and partial photo (b) of two-channel adaptive interferometer based on dynamic reflection holograms angularly multiplexed in PR crystal: PD1 and PD2 are phototdetectors which register signal beam intensities in 1st and 2nd channels

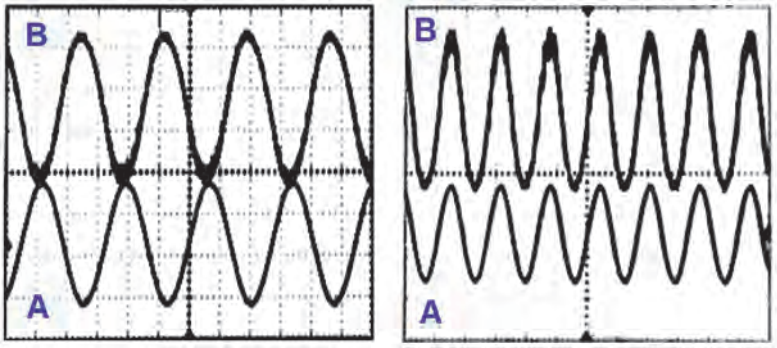

Fig. 17. Snapshots of oscilloscope traces demonstrating the operation of a two-channel adaptive measurement system: the first channel (left) and the second channel (right); (A) modulation signal which excites vibration in sensing fibers, (B) signal detected in a channel

6. Spectral multiplexing of dynamic holograms

Spectral (or wavelength division) multiplexing is one of effective techniques for building multichannel optical and fiber-optical measurement systems. In particular, this approach is highly demanded if fiber Bragg gratings (FBG) are used as sensors (Grattan & Meggitt, 1998). FBG sensors are an increasingly important emerging technology in the area of intelligent structural health monitoring (SHM) of civil, mechanical, naval, and aerospace structures (Claus, 1992; Culshaw & Dakin, 1996). A large number of FBG sensors can be easily written in a single fiber. A measurand (for SHM applications, FBG sensors are typically used to monitor static or dynamic strains) causes spectral shifts in the FBG sensor

transmittivity (equivalently reflectivity). The spectral shifts can be monitored in several ways with an appropriate demodulator. For spectrally encoded FBG sensors, extant demodulation schemes can be classified into three categories: scanning type, spectrometry based, and interferometry based. Scanning-type techniques include Fabry–Perot scanning filters (Kersey, et al., 1993), acoustooptic tunable filters (Xu, et al., 1993), and tunable laser sources (Fomitchov & Krishnaswamy, 2003). All these scanning-type techniques suffer from the fact that at any instant only one FBG sensor can be interrogated. Such approaches are not applicable if all the sensors have to be interrogated *simultaneously* for the purpose of monitoring impact signals and acoustic emissions (Perez, et al., 2001). Spectrometric methods (Davis & Kersey, 1995) suffer from low sensitivity and are not suitable for dynamic measurements if several sensors have to be active at all times. Interferometric methods such as the Mach–Zehnder interferometer (Kersey, et al., 1992) are ideally suited to monitor dynamic strains; however, they require electronic feedback to actively compensate for any quasi-static drift to maintain the interferometer at quadrature. This makes the cost of multiplexing high since each sensor requires its own feedback system. Therefore, a cost-effective multichannel demodulator capable of providing not only simultaneous interrogation of FBG-sensor arrays but also stable performance in unstable environment is required.

In the paper (Qiao, et al., 2006) authors show that such a demodulator can be developed on the basis of dynamic holograms formed in a photorefractive crystal. Consider this in more details.

Due to its adaptive properties a PRC-based demodulator can compensate all slow (including quasi-static) impacts on sensors and provide stable detection of high-frequency or pulse measurands (e.g., vibration, ultra-sonic waves, acoustic emission, etc.) without using any feedback loops or external stabilizing electronic circuits. As will be considered below, the demodulator based on two-wave mixing in a PR crystal can provide both spectral decoding of FBG-sensor signals and their effective spectral demultiplexing.

The spectral shift induced by strain, ε_F, and temperature change, ΔT, in a Bragg-grating sensor can be written as (Murray, et al., 2000):

$$\Delta\lambda_B = \lambda_B \left\{ 1 - \frac{n_{\text{eff}}^2}{2}\left[p_{12} - u(p_{11} + p_{12})\right]\varepsilon_F + (\alpha_T + \alpha_N)\Delta T \right\}, \tag{17}$$

where, λ_B is the center wavelength of the FBG sensor, $\Delta\lambda_B$, is the wavelength shift caused by strain or temperature, n_{eff} is the effective refractive index of the fiber, p_{ij} (i, j = 1, 2) are the components of the strainoptic tensor, u is Poisson's ratio, α_T is the thermal expansion coefficient, and α_N is the thermo-optic coefficient of the fiber. For typical Bragg sensors at 1550 nm, it has been estimated that one microstrain (1×10^{-6}) will lead to a 1.2 pm change in wavelength, and a 1 °C change in temperature will lead to about 13 pm change in wavelength (Othonos & Kalli, 1999). This fact emphasizes again the necessity of compensation for environment effects in the measurement system.

The adaptive interferometer based on dynamic holograms provides transformation of transient phase shift to intensity modulation of signal beam, while the signal of FBG-sensor is encrypted in a shift of central wavelengths in the reflection spectra. At the same time the adaptive interferometer also can be configured as a *spectral* demodulator. Indeed, a spectral shift $\Delta\lambda_B$ of the signal *and* reference beams can be effectively converted into a relative phase shift $\Delta\phi$ *between* the beams due to travel through unbalanced optical paths (Othonos & Kalli, 1999):

$$\Delta\phi(t) = \frac{2\pi b}{\lambda_B^2}\Delta\lambda_B, \tag{18}$$

where b is the optical path difference (OPD). It is noteworthy that a similar principle of spectra change transformation to phase modulation is used as well in Mach-Zehnder and other unbalanced interferometers (Kersey, et al., 1992).
From Eq. (18), it appears that the greater the OPD, the larger the equivalent phase shift, and therefore the stronger the interference signal should be. However, typically broadband light sources are used to illuminate the FBG sensors, and the FBG reflection spectrum typically has a finite line width of the order of 0.1–0.4 nm. This implies that coherence of the two interfering beams needs to be taken into account both in the photorefractive grating creating process, and in the subsequent interference between the transmitted signal and the diffracted reference beams. The fringe visibility due to the interference of two beams of finite spectral width Δk is given by

$$m(b) = \frac{2\sqrt{\beta}}{\beta+1}\exp\left\{-\frac{\Delta k^2 b^2}{16\ln 2}\right\}, \tag{19}$$

where β is the intensity ratio of reference and signal beams. The factor before *exp*-function in Eq.(19) is nothing other than interference fringe contrast m defining space charge field in PR crystal (see Eq.(2)). Incorporating the degradation in fringe visibility due to low coherence in the TWM analysis (by solving the coupled-wave equations) leads to the following expression for spectral-shift demodulated interference signal:

$$\Delta I_S \propto \left[\exp(\gamma' L)\sin(\gamma'' L)\right]\exp\left\{-\frac{\Delta k^2 b^2}{16\ln 2}\right\}\frac{b}{\lambda_B^2}\Delta\lambda_B, \tag{20}$$

where $\gamma = \gamma' + i\gamma''$ is the TWM complex gain and L is the crystal length in the beam propagation direction.
The effect of decreased fringe visibility on the photorefractive grating formation process is not a significant factor, since the preferred mode of two-wave mixing in PRCs is in the low intensity modulation regime (this avoids the creation of higher order index gratings that could lead to cross talk when the system is multiplexed). Furthermore, the system is operated at near quadrature, when $\gamma'' L \approx \pi/2$ (Solymar, et al., 1996), and since the TWM energy gain, γ', is typically very small, the variations in the first two terms with the OPD are not significant. The dependence of the interference signal on the OPD is therefore predominantly given by

$$\Delta I_S \propto \exp\left\{-\frac{\Delta k^2 b^2}{16\ln 2}\right\}\frac{b}{\lambda_B^2}\Delta\lambda_B. \tag{21}$$

As seen from Eq.(21), the wavelength demodulation signal is a strong function of the OPD d with the exponential decay arising from loss of coherence, and the linear increase arising from the increase with OPD in the phase shift due to spectral change. Figure 18 is a plot of the signal amplitude versus the OPD for different linewidth FBG sensors. As indicated in Fig. 18, when the OPD equals zero, there is no wavelength-demodulated signal detected,

and as the OPD increases the signal amplitude increases to a maximum beyond which the signal starts to drop due to decreasing fringe visibility. For each given line width of the FBG sensor, there exists an optimum value of the OPD that maximizes the wavelength-demodulated signal. It is also clear from Fig. 18 that the narrower the linewidth, the larger the optimum OPD, and therefore the larger the demodulated signal. However, it is not always better to use a narrower linewidth FBG sensor. First, a narrower linewidth FBG sensor is usually longer in length (Othonos & Kalli, 1999), which decreases the highest frequency to which the FBG can respond (Coppola, et al., 2001). Second, a larger OPD decreases the dynamic range that the FBG sensor can measure.

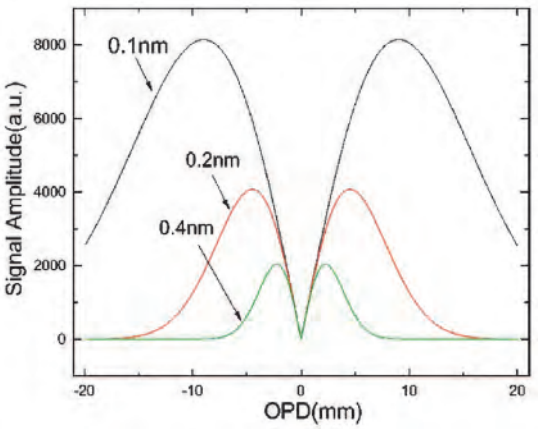

Fig. 18. Wavelength demodulated signal amplitude as a function of the OPD for different linewidth FBG sensors

The scheme of the measurement system based on FBG sensor and photorefractive dynamic hologram proposed in (Qiao, et al., 2006) is shown in Fig. 19. The FBG sensor is illuminated by a broadband amplified spontaneous emission (ASE) source in the C band (1530 to 1570 nm), and the reflected light is coupled by a circulator into an erbium-doped fiber amplifier (EDFA) that works in saturation mode (output 500 mW). The amplified light is split using a 1 × 2 coupler (splitting ratio 95/5) into reference (95%) and signal (5%) beams that travel unbalanced optical paths to the InP:Fe photorefractive crystal. The InP:Fe crystal is oriented for two-wave mixing in the direct detection configuration (Delaye, et al., 1997), in which both beams enter the crystal by the $(\bar{1}10)$ face. An external dc field (6 kV/cm) was applied along [001] direction to provide the quadrature condition of phase detection. The authors note that to apply a continuous dc field across the InP:Fe crystal, a Peltier cooler was used to prevent electrical breakdown due to crystal overheating.

In the work (Qiao, et al., 2006) a FBG sensor centered at 1552 nm with a linewidth of 0.1 nm, length of 10 mm, and reflectivity of 50% was glued onto a piezoelectric transducer (PZT) stretcher that was used to induce known dynamic strains (with amplitude 10 μstrain at frequency 10 kHz). The light reflected from the FBG sensor undergoes spectral shift due to strain-induced changes in the Bragg reflectivity. The sensor by itself is sensitive to both quasi-static and dynamic strains, and is also subject to temperature drift. However the TWM

demodulator system will automatically compensate for quasi-static drifts and track only the dynamic strains.

Oscilloscope traces of demodulated signal obtained at different values of the optical path difference are shown in Fig. 20. As seen, an intermittent dc field is applied from 1 to 6 ms with respect to a reference trigger, and the photorefractive grating initially builds up. The dynamic strain is applied as a tone burst starting from 2 to 6 ms. When the OPD equals to zero, although the TWM energy gain is at its maximum, there is no detected wavelength demodulated signal because there is no OPD to convert the wavelength shift into phase shift. As the OPD increases, the wavelength demodulated signal starts to appear.

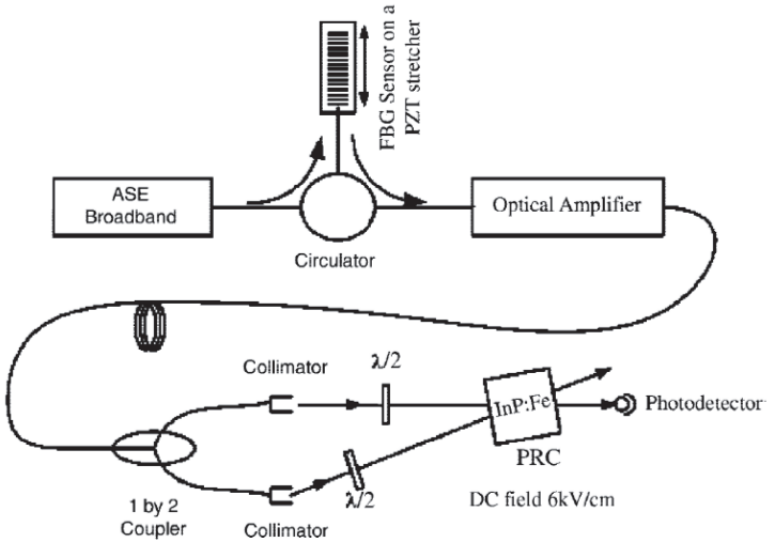

Fig. 19. Experimental configuration of the FBG sensor and the TWM wavelength demodulator

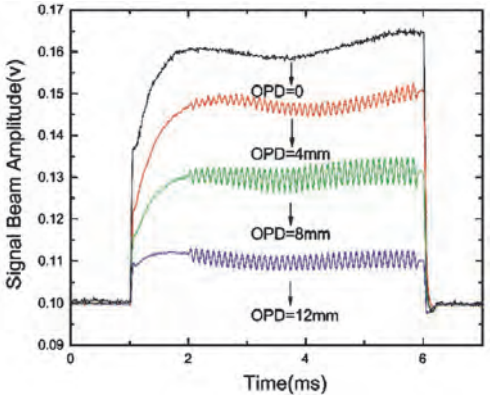

Fig. 20. Wavelength demodulated signal at different values of OPD

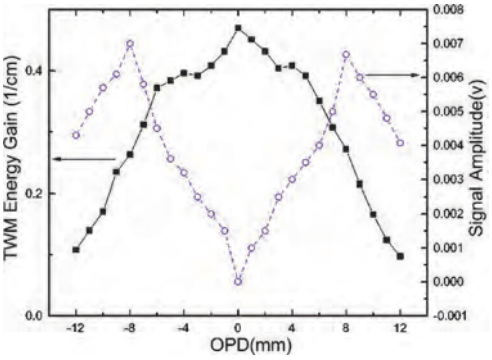

Fig. 21. Plot of wavelength demodulated signal amplitude and TWM gain versus OPD

Figure 21 is a plot of the wavelength demodulated signal amplitude and TWM energy gain versus the OPD. The optimum OPD that maximizes the wavelength demodulated signal for the 0.1 nm linewidth FBG sensor is found to be 8 mm. For an OPD of 8 mm, Eq. (18) indicates a wavelength-to-phase shift conversion sensitivity of about 21 radians per nanometer wavelength shift at 1550 nm wavelength. This translates to 0.0252 radian/με. Such phase shifts are readily detectable by the TWM interferometer. Also note that the trend of the signal amplitude curve is similar to that of the theoretical curve shown in Fig. 18. Also, as was mentioned above, the TWM energy gain γ' is indeed a small number and experimentally is found to vary from 0.47 to 0.1 cm^{-1} as the OPD changes from 0 to 12 mm. This causes the first exponential term in Eq. (20) to vary from 1.6 to 1.1, which is much smaller than the change in the second exponential term that decreases from 1 to 0.03.

The minimum detectable strain with the setup of adaptive interferometer proposed and realized in (Qiao, et al., 2006) was measured to be 0.25 με, corresponding to a spectral shift of 0.3 pm. The minimum detectable spectral shift, which is limited by the ASE source and EDFA intensity noise, can be further improved by using balanced photodetection to cancel the intensity noise.

Let us consider now how the multi-channel measurement system can be created on the basis of decoding of spectral signals from FBG sensors in PR crystal. The general principle is following (Qiao, et al., 2006). Optical signals from FBG sensors with distinct spectral reflectivities and center wavelength separation, $\Delta\lambda_C$, propagate in common optical path and enter a single PR crystal where they record a set of dynamic holograms which in its turn provides demodulation of spectrally encoded signals. Then the signals coming from different FBGs are separated by means of band-drop filters widely used in optical communication systems.

The distance between FBG central wavelengths $\Delta\lambda_C$ is chosen to be sufficiently large so that stationary optical interference between the multiple channels cannot occur. In this case, inside the PRC each channel creates its own index grating of different grating pitch. The change in the index grating pitch, $\Delta\Lambda$, is related to the channel separation and the signal and reference beam angle θ:

$$\Delta\Lambda = \frac{\Delta\lambda_C}{2\sin(\theta/2)}. \tag{22}$$

It is worth noting that the FBG channel spacing $\Delta\lambda_C$ should be neither too small to avoid cross talk due to closely packed index gratings, nor too large to maximize the number of sensors that can be used within the limited bandwidth of the light source and that of spectral sensitivity of the PR crystal. Thus, for the C band (1530–1570 nm), the channel separation $\Delta\lambda_C$ was 4 nm, which, according to Eq.(22), will give rise to an index grating pitch shift of 76 nm at a beam angle of 3°. In the context of holographic storage elements using PRCs, it has been shown that multiple gratings can be written in a single PRC with negligible cross talk if the grating pitches were to differ by as little as 0.03 nm (Kume, et al., 1998). Thus, a 4 nm channel spacing allows 10 channels with very small cross talk in the C band. In practice, this can be increased by using narrower channel spacing, at the expense of decreased dynamic range.

The experimental configuration of a four-channel TWM wavelength demodulator demonstrated in (Qiao, et al., 2006) is shown in Fig. 22. Four 0.1 nm linewidth FBG sensors are connected in series and are centered at 1548, 1552, 1556, and 1560 nm, respectively. The experimental configuration is similar to that of the single channel configuration shown in Fig. 19 except that after the PRC, there are four band-drop filters which transmit a certain band (i.e., from 1546.8 to 1549.4 nm) and reflect all the other wavelengths. The band-drop filters therefore decouple the TWM-demodulator signals from the various FBG sensors prior to photodetection. The width of the band-drop filter should be chosen to be wider than the expected quasi-static phase shifts of the FBG sensors, and to be slightly narrower than the FBG channel spacing $\Delta\lambda_C$.

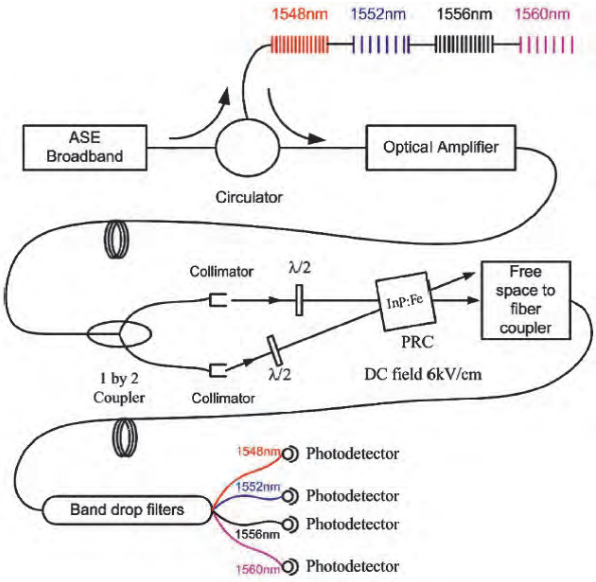

Fig. 22. Experimental configuration of the four-channel adaptive measurement system based on spectral multiplexing of FBG sensors and TWM demodulation of their signals at dynamic holograms in PRC

Performance of the four-channel adaptive measurement system is illustrated by Fig.23 which shows oscilloscope traces of demodulation signal in each channel of the system.

Dynamic strains with equal amplitude (5 με) and different frequencies were simultaneously applied to all FBG sensors: 10 kHz on FBG sensor 1 (1548 nm), 5 kHz on FBG sensor 2 (1552 nm), 2 kHz on FBG sensor 3 (1556 nm), and 20 kHz on FBG sensor 4 (1560 nm). Figure 23(a) shows that the four channels can be demodulated simultaneously. Note that the low frequency fluctuations seen in the signals are due to environmental noise-induced *intensity* fluctuations as explained earlier, and these can be removed using a balanced detection scheme if necessary. Also note that although the applied signal amplitudes for all four channels are the same, the demodulated signal amplitude for each channel is slightly different. This is mainly due to each channel having different optical intensities (due to nonuniform EDFA gain). In practice, this can either be precalibrated, or a gain-flattened EDFA can be used.

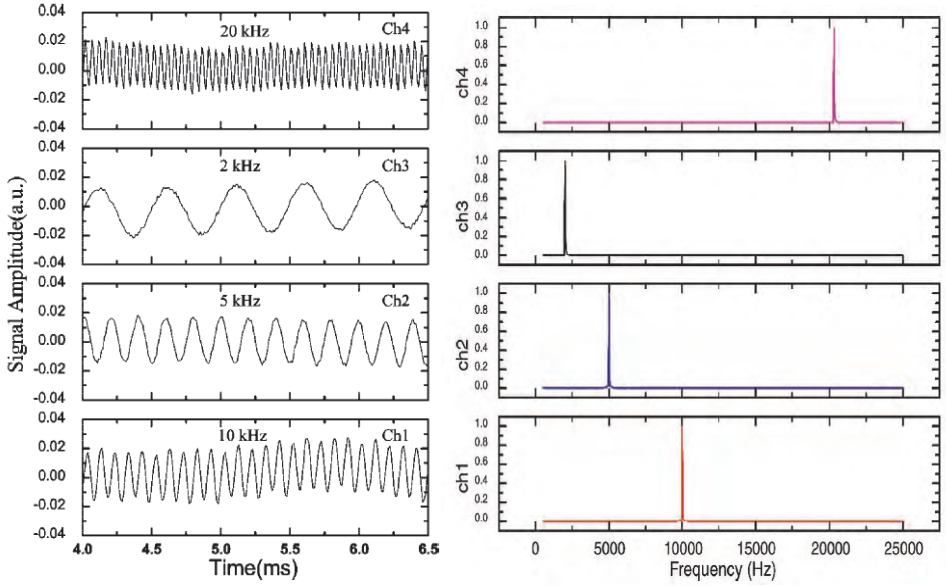

Fig. 23. Output demodulated signals (a) and their Fourier spectra (b) in four channels of adaptive measurement system based on FBG sensors and dynamic holograms spectrally multiplexed in PR crystal

The cross talk between these four channels can be inferred from the Fourier spectra of the signals shown in Fig.23(b). If there were cross talk, we would expect all the frequency components, namely 2, 5, 10, and 20 kHz, to show up in the signal spectrum of each channel. However, in the spectrum of channel 1, there is only the expected 10 kHz component, and no other frequency components are observed. This is true also for the other three channels. It is safe to conclude that the cross talk between these four channels is at most comparable to the noise level in the Fourier spectrum, which is at least 30 dB below the signal level in this particular case.

To conclude this Section we note that, apart from band-drop filters with fixed central wavelengths used in the paper (Qiao, et al., 2006), other WDM-demultiplexers including

those of scanning type can be used for spectral division of channels. Note as well that such a demultiplexer can be also built on the basis of dynamic holographic grating recorded in a PR crystal (Hukriede, et al., 2003; Petrov, et al., 2001; Petrov, et al., 2003; Runde, et al., 2005).
The scheme of such photorefractive band-drop filter proposed in (Petrov, et al., 2003) is shown in Fig. 24. Two coherent light beams A and B (λ_w = 532 nm) making the angle 2θ enter the photorefractive crystal $BaTiO_3$:Co where they form a dynamic holographic grating with the index pitch $\Lambda_F = \lambda_w/(2\sin\theta)$. Radiation to be spectrally filtered enters the crystal along the wave vector of holographic grating $\mathbf{K_F}$ (see Fig. 24) which acts as a Bragg mirror with central wavelength

$$\lambda_B = \frac{n_C \lambda_w}{\sin\theta}, \tag{23}$$

where n_C is the refractive index of crystal.
Figure 25 shows typical transmission spectrum of band-drop filter based on a holographic grating formed in PRC. As seen, the filter has high Q-factor due to narrow line width ~0.1 nm.

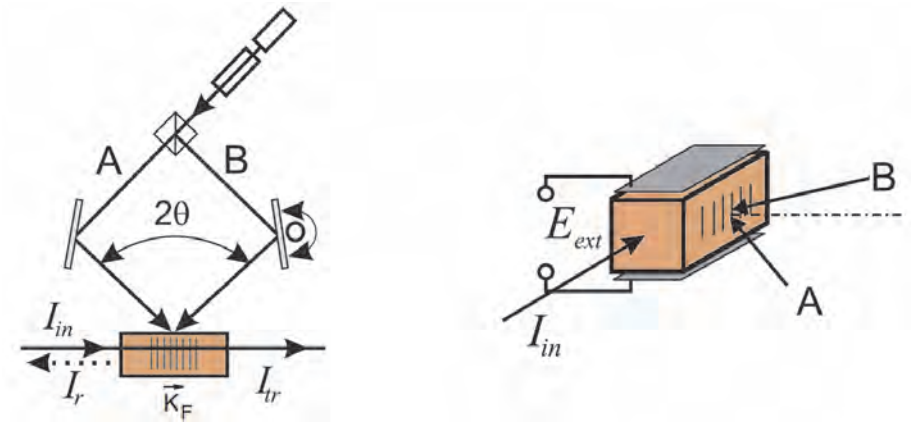

(a) (b)

Fig. 24. Geometry of dynamic band-drop Bragg filter recording in PR crystal (a) and orientation of external electric field applied to a crystal (b)

The adaptive property of a dynamic grating formed in PRC allows one to perform fine tuning of the filter parameter thus providing on-line switching between different FBG sensors. Thus, change of the angle θ between recording beams leads to erasure of the previous grating and recording of a new one with new pitch corresponded to new central wavelength λ_B. As seen from Fig. 26 which shows experimental dependence of central wavelength on the angle θ, the change of the latter leads to shift of λ_B by 80 nm (from 1480 to 1560 nm). Authors (Petrov, et al., 2003) note that shift of the Bragg wavelength has no observable effect on the form of the transfer function and the diffraction efficiency. The speed of tuning was determined by the recording time of the dynamic hologram and was about 0.5 s.

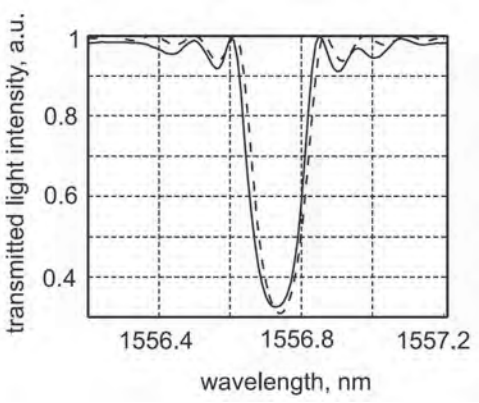

Fig. 25. The transfer function of the simple dynamic Bragg grating

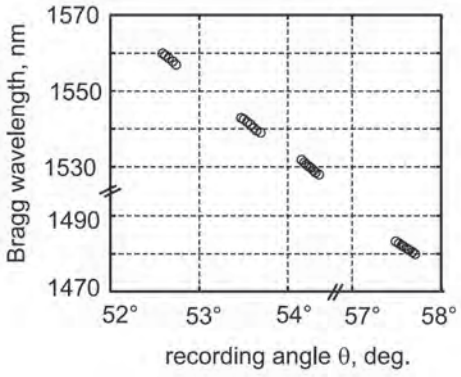

Fig. 26. The wavelength position of the filter transfer function versus the angle θ between the writing beams

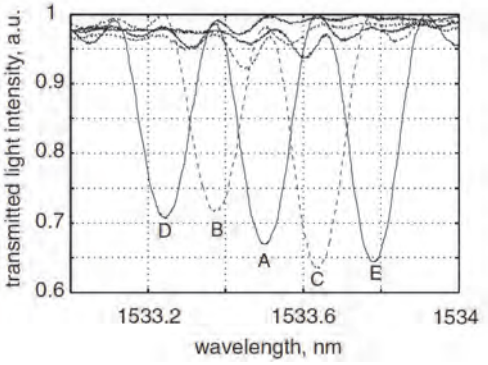

Fig. 27. The wavelength position of the filter transfer function versus the external electric field: A, E_{ext} = 0; B, E_{ext} = −370 V cm^{-1}; C, E_{ext} = +389 V cm^{-1}; D, E_{ext} = −614 V cm^{-1}; E, E_{ext} = +653 V cm^{-1}

The central wavelength of the filter based on a photorefractive grating can be additionally tuned electrically by application of external electric field to the photorefractive crystal. Figure 27 demonstrates such electrical tuning of the filter. This is an example of fast tuning via the electro-optically induced variations in the average refractive index. One can see that the application of voltages ranging from −614 to +655 V cm^{-1} provides tuning in the 0.55 nm range. The speed of tuning reached 2.2 nm μs^{-1} and was limited only by the available equipment (e.g. switching time of the power source used).

7. Conclusion

In this Chapter we considered different approaches to development of multi-channel adaptive measurement systems based on multiplexing of dynamic holograms in a photorefractive crystal. We show that such systems can provide (i) high sensitivity to detection of ultra-small physical quantities (close to the classical homodyne detection limit), (ii) cross-talk free performance, and (iii) adaptive properties which cancel uncontrollable environmental influence on the system. For development of such systems different approaches to dynamic holograms multiplexing, including spatial, angular, spectral and their combinations, can be effectively used. Moreover, dynamic gratings recorded in a photorefractive crystal can also be used for development of such elements of multi-channel systems as spectral tunable filters which can provide effective demultiplexing of signals with different wavelengths.

8. References

An, J. W.; Kim, N. and Lee, K. W. (2001). Volume holographic wavelength demultiplexer based on rotation multiplexing in the 90-deg geometry. *Opt. Comm.*, Vol.197, pp.247-254, ISSN 0030-4018

Andersen, G. P.; Dussan, L. and Chen, K. (2009). Holographic wavefront sensor. *Opt. Eng.*, Vol.48, No.8, p.085801, ISSN 0091-3286

Ashkin, A.; Boyd, G. D.; Dziedzic, J. M.; Smith, R. G.; Ballman, A. A.; Levinstein, J. J. and Nassau, K. (1966). Optically-induced refractive index inhomogeneities in $LiNbO_3$ and $LiTaO_3$. *Appl. Phys. Lett.*, Vol.9, No.1, pp.72-74, ISSN 0003-6951

Bershtein, I. L. (1954). Measurement of extremely small changes of path difference of two light oscillations. *Dokl. Acad. Nauk USSR*, Vol.94, No.4, pp.655-658

Claus, R. O. (Ed). (1992). *Fiber Optic Sensor Based Smart Materials and Structures*. Institute of Physics Publishing, ISBN 0-7503-0248-8, Bristol

Coppola, G.; Minardo, A.; Cusano, A.; Breglio, G.; Zeni, G.; Cutolo, A.; Calabro, A.; Giordano, M. and Nicolais, L. (2001). Analysis of feasibility on the use of fiber Bragg grating sensors as ultrasound detectors, *Proceedings of SPIE "Smart Structures and Materials 2001"*, Vol.4328, Febraury, 2001

Cronin-Golomb, M. and Yariv, A. (1985). Optical limiters using photorefractive nonlinearities. *J. Appl. Phys.*, Vol.57, No.11, pp.4906-4910, ISSN ISSN 0021-8979

Culshaw, B. and Dakin, J. (Eds). (1996). *Optical Fiber Sensors. Applications, Analysis, and Future Trends*. Artech House, London

Davis, M. A. and Kersey, A. D. (1995). Application of a fiber Fourier transform spectrometer to the detection of wavelength encoded signals from Bragg-grating sensors. *J. Lightwave Technol.*, Vol.13, pp.1289-1295, ISSN 0733-8724

Delaye, P.; Blouin, A.; Drolet, D.; de Montmorillon, L.-A.; Roosen, G. and Monchalin, J.-P. (1997). Detection of ultrasonic motion of a scattering surface using photorefractive InP:Fe under an applied dc field. *J. Opt. Soc. Am. B*, Vol.14, No.7, pp.1723-1734, ISSN 1520-8540

Delaye, P.; Roosen, G.; Ramaz, F.; Forget, B. C.; Atlan, M.; Boccara, A. C. and Gross, M. (2005). Photorefractive two wave mixing detection for acousto-optical imaging of biological thick tissues, *Proceedings of 10th Int. Conf. on Photorefractive Effects, Materials, and Devices PR-05*, Vol.99, Sanya, Hainan, China, 19-23 July, 2005

de Montmorillon, L.-A.; Delaye, P.; Launay, J.-C. and Roosen, G. (1997). Novel theoretical aspects on photorefractive ultrasonic detection and implementation of a sensor with an optimum sensitivity. *J. Appl. Phys.*, Vol.82, No.12, pp.5913-5922, ISSN 1089-7550

Dewhurst, R. J. and Shan, Q. (1999). Optical remote measurement of ultrasound. *Meas. Sci. Technol.*, Vol.10, pp.R139-R168 ISSN 0957-0233

Di Girolamo, S.; Kamshilin, A. A.; Romashko, R. V.; Kulchin, Y. N. and Launay, J.-C. (2007a). Fast adaptive interferometer on dynamic reflection hologram in CdTe:V. *Opt. Express*, Vol.15, No.2, pp.545-555, ISSN 1094-4087

Di Girolamo, S.; Kamshilin, A. A.; Romashko, R. V.; Kulchin, Y. N. and Launay, J.-C. (2007b). Sensing of multimode-fiber strain by a dynamic photorefractive hologram. *Opt. Lett.*, Vol.32, No.13, pp.1821-1823, ISSN 0146-9592

Di Girolamo, S.; Romashko, R. V.; Kulchin, Y. N.; Launay, J.-C. and Kamshilin, A. A. (2008). Fiber sensors multiplexing using vectorial wave mixing in a photorefractive crystal. *Opt. Express*, Vol.16, No.22, pp.18041-18049, ISSN 1094-4087

Di Girolamo, S.; Romashko, R. V.; Kulchin, Y. N. and Kamshilin, A. A. (2010). Orthogonal geometry of wave interaction in a photorefractive crystal for linear phase demodulation. *Opt. Comm.*, Vol.283, pp.128-131, ISSN 0030-4018

Feinberg, J. (1982). Asymmetric self-defocusing of an optical beam from the photorefractive effect. *J. Opt. Soc. Am.*, Vol.72, No.1, pp.46-51

Feng, W.; Yan, Y.; Jin, G.; Wu, M. and He, Q. (2000). Multiplexing of volume holographic wavelet correlation processor. *Opt. Comm.*, Vol.176, pp.49-59, ISSN 0030-4018

Fomitchov, P. A.; Kim, Y. K.; Kromin, A.; Krishnaswamy, S.; Achenbach, J. D. and Daniel, I. M. (2001). Distributed photoacoustic system for cure monitoring of composites, *Proceedings of SPIE "Advanced Nondestructive Evaluation for Structural and Biological Health Monitoring"*, Vol.4335, July, 2001

Fomitchov, P. A.; Murray, T. W. and Krishnaswamy, S. (2002). Intrinsic fiber-optic ultrasonic sensor array using multiplexed two-wave mixing interferometry. *Appl. Opt.*, Vol.41, No.7, pp.1262-1266, ISSN 1559-128X

Fomitchov, P. A. and Krishnaswamy, S. (2003). Response of a fiber Bragg-grating ultrasound sensor. *Opt. Eng.*, Vol.42, pp.956-963, ISSN 0091-3286

Forward, R. L. (1978). Wideband laser-interferometer graviational-radiation experiment. *Phys. Rev.*, Vol.17, No.2, pp.379-390

Grattan, K. T. V. and Meggitt, B. T. (Eds). (1998). *Optical Fiber Sensor Technology: Devices and Technology*. Chapman and Hall, ISBN 0-412-78290-1, London

Hall, T. J., Fiddy, M. A. and Ner, M. S. (1980). Detector for an optical-fiber acoustic sensor using dynamic holographic interferometry. *Opt. Lett.*, Vol.5, No.11, pp.485-487, ISSN 0146-9592

Hariharan, P. (1990). Optical interferometry. *Rep. Prog. Phys.*, Vol.54, No.3, pp.339-390, ISSN 0034-4885

Huignard, J. P. and Marrakchi, A. (1981). Two wave mixing and energy transfer in $Bi_{12}SiO_{20}$ crystals: application to image amplification and vibration analysis. *Opt. Lett.*, Vol.6, No.12, pp.622-624, ISSN 0146-9592

Hukriede, J.; Runde, D. and Kip, D. (2003). Fabication and application of holographic Bragg gratings in photorefractive lithium niobate channel waveguides. *J. Phys. D: Appl. Phys.*, Vol.36, pp.R1-R16, ISSN 1361-6463

Kamshilin, A. A.; Frejlich, J. and Cescato, L. (1986). Photorefractive crystals for the stabilization of the holographic setup. *Appl. Opt.*, Vol.25, No.14, pp.2375-2381, ISSN 1559-128X

Kamshilin, A. A.; Jaaskelainen, T.; Khomenko, A. V. and Garcia-Weidner, A. (1995). Multimode fiber-optic sensor using photorefractive double phase conjugator. *Appl. Phys. Lett.*, Vol.67, No.18, pp.2585-2587, ISSN 0003-6951

Kamshilin, A. A.; Jaaskelainen, T. and Kulchin, Y. N. (1998). Adaptive correlation filter for stabilization of interference-fiber-optic sensors. *Appl. Phys. Lett.*, Vol.73, No.6, pp.705-707, ISSN 0003-6951

Kamshilin, A. A. and Grachev, A. I. (2002). Adaptive interferometer based on wave mixing in a photorefractive crystal under alternating electric field. *Appl. Phys. Lett.*, Vol.81, No.16, pp.2923-2925, ISSN 0003-6951

Kamshilin, A. A.; Romashko, R. V. and Kulchin, Y. N. (2009). Adaptive interferometry with photorefractive crystals. *J. Appl. Phys.*, Vol.105, pp.031101(11), ISSN 0021-8979

Kersey, A. D.; Berkoff, T. A. and Morey, W. W. (1992). High resolution fiber-grating based strain sensor with interferometric wavelength shift detection. *Electron. Lett.*, Vol.28, pp.236-238, ISSN 0013-5194

Kersey, A. D.; Berkoff, T. A. and Morey, W. W. (1993). Multiplexed fiber Bragg grating strain-sensor system with a Fabry–Perot wavelength filter. *Opt. Lett.*, Vol.18, pp.1370-1372, ISSN 0146-9592

Kujawinska, M. and Robinson, D. W. (1988). Multichannel phase-stepped holographic interferometry. *Appl. Opt.*, Vol.27, No.2, pp.312-320, ISSN 1559-128X

Kukhtarev, N. V.; Markov, V. B.; Odulov, S. G.; Soskin, M. S. and Vinetskii, V. L. (1979). Holographic storage in electrooptic crystals. I. Steady state. *Ferroelectrics*, Vol.22, pp.949-960, ISSN 0015-0193

Kulchin, Y. N.; Romashko, R. V. and Piskunov, E. N. (2000a). Multi-channel adaptive fiber-optical system for monitoring of fast processes in solid state, *Proceedings of SPIE "Asia-Pacific Conference on Fundamental Problems of Opto- and Microelectronics APCOM-2000"*, Vol.4513, Vladivostok, Russia, September, 2000

Kulchin, Y. N.; Romashko, R. V.; Piskunov, E. N. and Kamshilin, A. A. (2000b). A multichannel correlation filter based on a photorefractive crystal for the processing of varying speckle fields. *Tech. Phys. Lett.*, Vol.26, No.6, pp.505-507, ISSN 1063-7850

Kulchin, Y. N. (2001). *Distributed Fiber-Optical Measurement Systems*, Fizmatlit, ISBN 978-5-9221-0072-4, Moscow, Russia

Kume, T.; Nonaka, K.; Yamamoto, M. and Yagi, S. (1998). Wavelength-multiplexed holographic data storage by use of reflection geometry with a cerium-doped strontium bariumniobate single-crystal structure and a tunable laser diode. *Appl. Opt.*, Vol.37, pp.334-339, ISSN 1559-128X

Lichtenberg, S.; Heinisch, S.; Petrov, V. M.; Petter, J. and Tschudi, T. (2005). Refractive index measurement using an adaptive interferometer based on phase-shift keying, *Proceedings of 10th Int. Conf. on Photorefractive Effects, Materials, and Devices PR-05*, Vol.99, Sanya, Hainan, China, 19-23 July, 2005

Murray, T. W.; Tuovinen, H. and Krishnaswamy, S. (2000). Adaptive optical array receivers for detection of surface acoustic waves. *Appl. Opt.*, Vol.39, No.19, pp.3276-3284, ISSN 1559-128X

Osterberg, H. (1932). An interferometer method of studying the vibrations of an oscillating quartz plate. *J. Opt. Soc. Am.*, Vol.22, No.1, pp.19-35

Othonos, A. and Kalli, K. (1999). *Fiber Bragg Gratings: Fundamentals and Applications in Telecommunications and Sensing*, Artech House Publishers, ISBN 978-0890063446

Pauliat, G.; Roosen, G.; Georges, M. P. and Pedrini, G. (2006). Passive introduction of carrier fringes in real-time photorefractive interferometers for single interferogram analysis. *J. Europ. Opt. Soc.*, Vol.1, p.06024, ISSN 1990-2573

Peiponen, K. E.; Myllylä, R. and Priezzhev, A. V. (2009). *Optical Measurement Techniques*, Springer, ISBN 978-3-540-71926-7, Berlin

Peng, L.; Varma, M. M.; Regnier, F. E. and Nolte, D. D. (2007). Adaptive interferometry of protein on a BioCD. *Appl. Opt.*, Vol.46, No.22, pp.5384-5395, ISSN 1559-128X

Peng, L.; Yu, P.; Nolte, D. D. and Melloch, M. R. (2003). High-speed adaptive interferometer for optical coherence-domain reflectometry through turbid media. *Opt.Lett.*, Vol.28, No.6, pp.396-398, ISSN 0146-9592

Perez, I.; Cui, H. and Udd, E. (2001). *Proceedings of SPIE "Smart Structures and Materials 2001"*, Vol.4328, Febraury, 2001

Petrov, M. P.; Stepanov, S. I. and Khomenko, A. V. (1983). *Photosensitive Electrooptic Materials in Holography and Optical Information Processing*, Nauka, Leningrad

Petrov, M. P.; Stepanov, S. I. and Khomenko, A. V. (1991). *Photorefractive Crystals in Coherent Optical Systems*, Springer-Verlag, ISBN 3-540-52603-X, Berlin, Germany

Petrov, V. M.; Denz, C.; Shamray, A. V.; Petrov, M. P. and Tschudi, T. (2001). Electrically controlled volume $LiNbO_3$ holograms for wavelength demultiplexing systems. *Optical Materials*, Vol.18, No.1, pp.191-194, ISSN 0925-3467

Petrov, V. M.; Lichtenberg, S.; Petter, J.; Tschudi, T.; Chamray, A. V.; Bryskin, V. V. and Petrov, M. P. (2003). Optical on-line controllable filters based on photorefractive crystals. *J. Opt. A: Pure Appl. Opt.*, Vol.5, pp.S471-S476, ISSN 1464-4258

Qiao, Y.; Zhou, Y. and Krishnaswamy, S. (2006). Adaptive demodulation of dynamic signals from fiber Bragg gratings using two-wave mixing technology. *Appl. Opt.*, Vol.45, No.21, pp.5132-5142, ISSN 1559-128X

Romashko, R. V.; Kulchin, Y. N. and Kamshilin, A. A. (2005a). Linear phase demodulation via reflection photorefractive holograms, *Proceedings of 10th Int. Conf. on Photorefractive Effects, Materials, and Devices PR-05*, Vol.99, Sanya, Hainan, China, 19-23 July, 2005

Romashko, R. V.; Kulchin, Y. N.; Shandarov, S. M.; Kargin, Y. F. and Volkov, V. V. (2005b). Adaptive correlation filter based on dynamic reflection hologram formed in photorefractive $Bi_{12}TiO_{20}$ crystal. *Opt. Rev.*, Vol.12, No.1, pp.59-60, ISSN 1340-6000

Romashko, R. V.; Kulchin, Y. N. and Kamshilin, A. A. (2007). Optimal geometry for fast and efficient hologram recording in photorefractive crystal. *Opt. Rev.*, Vol.14, No.4, pp.176-179, ISSN 1340-6000

Romashko, R. V.; Di Giloramo, S.; Kulchin, Y. N. and Kamshilin, A. A. (2010). Photorefractive vectorial wave mixing in different geometries. *J. Opt. Soc. Am. B*, Vol.27, No.2, pp.311-317, ISSN 1520-8540

Runde, D.; Breuer, S. and Kip, D. (2005). Holographic refelection filters in photorefractive LiNbO3 channel waveguides for applications as add/drop multiplexers, *Proceedings of 10th Int. Conf. on Photorefractive Effects, Materials, and Devices PR-05 (OSA Trends in Optics and Photonics)*, Vol.99, Sanya, Hainan, China, June, 2005

Solymar, L.; Webb, D. J. and Grunnet-Jepsen, A. (1996). *The Physics and Application of Photorefractive Materials*, Clarendon Press, Oxford

Steckman, G. J.; Pu, A. and Psaltis, D. (2001). Storage density of shift-multiplexed holographic memory. *Appl. Opt.*, Vol.40, No.20, pp.3387-3394, ISSN 1559-128X

Stepanov, S. I. (1991). Adaptive interferometry: a new area of applications of photorefractive crystals, In: *International Trends in Optics*, J.W. Goodman, (Ed.), pp.125-140, Academic Press, Inc., ISBN 0-12-289690-4, New York, London

Sturman, B. I. and Fridkin, V. M. (1992). *The Photovoltaic and Photorefractive Effect in Noncentrosymmetric Materials*, Gordon and Breach, ISBN 978-2-88124-498-8, New York, USA

Sturman, B. I.; Podivilov, E. V.; Ringhofer, K. H.; Shamonina, E.; Kamenov, V. P.; Nippolainen, E.; Prokofiev, V. V. and Kamshilin, A. A. (1999). Theory of photorefractive vectorial wave coupling in cubic crystals. *Phys. Rev. E*, Vol.60, No.3, pp.3332-3352, ISSN 0031-9007

Thizy, C.; Georges, M. P.; Kouloumpi, E.; Green, T.; Hackney, S. and Tornari, V. (2007). Photorefractive holographic interferometry for movable artwork assessment, *Proceedings of OSA Topical Meeting "Controlling light with light: Photorefractive Effects, Photosensitivity, Fiber Gratings, Photonic Materials and More"*, October, 2007

Voronov, V. V.; Dorosh, I. R.; Kuzminov, Y. S. and Tkachenko, N. V. (1980). Photoinduced light scattering in cerium-doped barium strontium niobate crystals. *Sov. J. Quantum Electron.*, Vol.10, No.11, pp.1346-1349, ISSN 0049-1748

Wagner, J. W. and Spicer, J. B. (1987). Theoretical noise-limited sensitivity of classical interferometry. *J. Opt. Soc. Am. B*, Vol.4, No.8, pp.1316-1326, ISSN 1520-8540

Wen, Z. and Yang, X. (1997). Multichannel photorefractive correlator for rotation-invariant optical pattern recognition. *Opt. Comm.*, Vol.135, pp.212-216, ISSN 0030-4018

Xu, M., Geiger, G. H. and Dakin, J. P. (1993). Modeling and performance nalysis of a fiber Bragg grating interrogation system using an acousto-optic tunable filter. *J. Lightwave Technol.*, Vol.14, No.391, p.396, ISSN 0733-8724

Young, L., Wong, W. K., Thewalt, M. L. and Cornish, W. D. (1974). Theory of formation of phase holograms in lithium niobate. *Appl. Phys. Lett.*, Vol.24, No.6, pp.264-265, ISSN 0003-6951